

Manuscript Template

FRONT MATTE	ER
-------------	----

3 4

1

Title: Direct detection of human adenovirus and SARS-CoV-2 with ability to inform infectivity using a DNA aptamer-nanopore sensor

5 6 7

Authors: Ana S. Peinetti, ^{1,†} Ryan J. Lake, ¹ Wen Cong, ² Laura Cooper, ³ Yuting Wu, ¹ Yuan Ma, ¹ Gregory T. Pawel, ¹ María Eugenia Toimil-Molares, ^{4,*} Christina Trautmann, ^{4,5} Lijun Rong, ^{3,*} Benito Mariñas, ^{2,*} Omar Azzaroni, ^{6,*} and Yi Lu^{1,*}

9 10

11

8

Affiliations

- ¹ Department of Chemistry, University of Illinois at Urbana-Champaign, Urbana, Illinois 61801,
- 13 United States.
- ² Department of Civil and Environmental Engineering, Safe Global Water Institute, University of
- 15 Illinois at Urbana-Champaign, Urbana, Illinois 61801, United States.
- ³ Department of Microbiology and Immunology, College of Medicine, University of Illinois at
- 17 Chicago, Chicago, Illinois 60612, United States
- ⁴ GSI Helmholtzzentrum für Schwerionenforschung, Darmstadt 64291, Germany.
- ⁵ Technische Universitat Darmstadt, Darmstadt 64287, Germany.
- ⁶ Instituto de Investigaciones Fisicoquímicas Teóricas y Aplicadas (INIFTA), Departamento de
- 21 Química, Facultad de Ciencias Exactas, Universidad Nacional de La Plata (UNLP), CONICET,
- Boulevard 113 y 64, La Plata 1900, Argentina.
- *Correspondence to: yi-lu@illinois.edu; azzaroni@inifta.unlp.edu.ar; marinas@illinois.edu;
- 24 lijun@uic.edu, m.e.toimilmolares@gsi.de
- [†]Current Address: INQUIMAE (CONICET), Departamento de Química Inorgánica, Analítica y
- 26 Química Física, Facultad de Ciencias Exactas y Naturales, Universidad de Buenos Aires, Ciudad
- 27 Universitaria, Pabellón 2, C1428EHA, Buenos Aires, Argentina

28 29

Abstract

- Viral infections are a major global health issue, but no current method allows rapid, direct, and
- ultrasensitive quantification of intact viruses with the ability to inform infectivity, causing misdiagnoses and spread of the viruses. Here, we report a method for direct detection and
- differentiation of infectious from noninfectious human adenovirus and SARS-CoV-2, as well as
- from other virus types, without any sample pretreatment. DNA aptamers are selected from a DNA
- library to bind intact infectious, but not noninfectious virus, and then incorporated into a solid state
- nanopore, which allows strong confinement of the virus to enhance sensitivity down to 1 pfu/mL
- for human adenovirus and 1×10^4 copies/mL for SARS-CoV-2. Our method matches the gold
- standard of plaque assay for direct viral detection that can inform infectivity, while taking much
- shorter time to obtain results and detecting viruses that are not culturable by the plaque assay.

 Applications of the aptamer-nanopore sensors in different types of water samples, saliva, and serum
- 41 are demonstrated for both enveloped and non-enveloped viruses, making the sensor generally

applicable for detecting these and other emerging viruses of environmental and public health concern.

Teaser

42 43

44

45

46 47

48 49

50 51

52

53

54

55

56

57

58

59

60

61

62

63

64

65

66

67

68

69

70

71

72

73 74

75

76

77

78

79

80

81

82

83 84

85

86 87

88

89

A novel sensor that can not only detect human adenovirus and SARS-CoV-2 in real world samples but also tell if they are infectious or not.

MAIN TEXT

Introduction

Viral infections are an important public health issue, as viral outbreaks, such as the recent COVID-19 pandemic, have resulted in enormous economic and societal impacts around the world. Critical to addressing this issue is timely and accurate viral diagnosis in both biological and environmental samples to enable the prompt treatment of viral infections while preventing the spread of viruses. It is thus important to develop a method that can rapidly detect virus particles at extremely low levels in complex samples (1) and without sample pretreatment to minimize false negative and false positive results. Of the widely used existing viral detection methods, viral nucleic acid detection with quantitative polymerase chain reaction (qPCR) has become the reference standard method due to its high sensitivity. However, this detection process requires long analysis time and expensive laboratory instruments, which limits its speed and availability. Other nucleic acid detection methods have been developed to address some of these issues to make tests based on genome detection more portable and accessible (2, 3). However, they still generally require sample pretreatment to extract the viral RNA and equipment to control the temperature during amplification (4). Alternatively, serological tests that detect antibodies (5) or immuno-tests that detect antigens (6) have shown potential to provide results at faster speed and requiring less sample pretreatment. However, antibodies produced in patients can only be detected 1-2 weeks after disease onset as opposed to viral RNA, which can be detected within the first few days (7). As such, serological tests are generally not suitable for viral disease diagnosis. Additionally, direct antigen detection generally has lower specificity and sensitivity compared to the nucleic acid-based tests (8).

Most critically, none of the current COVID-19 tests are able to differentiate infectious from noninfectious viruses, because the detection of viral nucleic acids, patient antibodies, or antigens alone does not indicate that intact infectious virus is present and levels of these biomarkers have shown poor correlation with infectivity (9). For instance, it has been shown that the SARS-CoV-2 viral RNA can remain detectable in some patients for more than 1 month after onset of illness, while viable virus could not be detected by culture after week 3 (10). In addition, viruses present in environmental samples, such as in air, water, or on different surfaces, can also be a major route for spreading infection. However, tests which are based on detection of viral nucleic acids or proteins cannot determine if the virus has been rendered noninfectious (inactivated) or is still infectious (active). The gold standard method for direct detection of viruses that can inform infectivity continues to be microbiology techniques, namely: plaque assays, however, it takes several days to grow plaques and requires growing the virus within host cells, which increases the required labor, expertise, and equipment and will not work for viruses that do not replicate well in cell culture systems (11). Therefore, despite many years of research and numerous publications, no existing method can allow direct and ultrasensitive detection and quantification of intact viruses with the ability to inform on infectivity. As a result, misdiagnoses and delayed treatment continue to occur daily and worldwide, especially given the fact that many asymptomatic people can transmit viruses unknowingly, which can result in further spread of viral disease.

To overcome the limitations of current methods, we herein report an efficient method for direct detection of intact viruses without sample pretreatment, with the ability to differentiate infectious from noninfectious viruses and to reach low detection limits. Our method integrates a highly selective DNA aptamer with a highly sensitive solid-state nanopore to selectively detect infectious viruses in both biological and environmental samples. This aptamer-nanopore sensor has been demonstrated for both human adenovirus (HAdV), which is a non-enveloped dsDNA virus that is responsible for respiratory water-borne diseases that especially affect children worldwide (12); and also a SARS-CoV-2 pseudotyped virus that incorporates the spike (S) protein of SARS-CoV-2 into a lentivirus, which mimic the surface of the native SARS-CoV-2, the novel enveloped ssRNA coronavirus that is responsible for the current COVID-19 pandemic. The wide diversity in viruses that our sensor can detect, both in terms of viral genome and envelope type, demonstrates that our method is generally applicable to a wide range of current and future emerging viruses.

Results

90

91

92

93

94 95

96 97

98 99

100

105

106

107

108

109

110

111

112

113

114

115

116

117

118

119

120

121

122

123

124

125

126

127

128

129 130

131

132

133

134

135136

137

138

139

To assess the infectivity of a virus, a major challenge is finding a sensing molecule that can bind and selectively recognize intact infectious viruses, and differentiate it from both the same virus that has been rendered noninfectious and also from other viruses. To meet this challenge, we utilized DNA aptamers as the recognition agent to selectively bind to an intact infectious virus. These DNA aptamers are DNA molecules with a specific sequence that allow them to form a specific 3D shape that can recognize a certain target with high affinity and selectivity that rivals antibodies and yet are less expensive and more stable (13). They can be obtained synthetically in a test tube using a combinatorial selection technique called systematic evolution of ligands by exponential enrichment (SELEX) or in vitro selection, in which sequences with high affinity are enriched from a DNA library of 10¹⁵ random sequences. Multiple selection rounds can be performed to gradually enrich the pool, with PCR amplification used in between rounds to restore the amount of DNA before each subsequent round. Additionally, the conditions for SELEX can be tailor-made to remove competing targets from known interfering species using counter selection (14). For the first selection target, HAdV, we designed the SELEX to include both positive selection steps to retain any DNA molecules that bind to infectious HAdV, and counter selection steps to discard any DNA sequences that bind to the same HAdV that had been rendered noninfectious by free chlorine treatment (15). A schematic representation of the selection process is shown in Fig. 1A, and details of the positive and counter selections are given in Methods section and Table 1. Additionally, SELEX was performed using the whole virus as the target, instead of a specific biomarker for the virus, such as a viral surface protein. In doing so, we aimed to select aptamers that will bind to the target in its native state, without the need for disruption of the virus (16–19). This method thus allows us to obtain recognition agents based on functional differences of the virus surface, which do not need to be known in advance. This ability is especially advantageous for the specific detection of infectious viruses, since the specific differences between infectious and noninfectious viruses, such as those rendered noninfectious through decontamination of surfaces or by the immune system in the body, is often not clearly understood, so SELEX is one of the only methods to obtain infectivity-specific recognition agents without any such foreknowledge of these differences. It has been reported that free chlorination treatment produces chemical modification on different residues of the protein on the surface of the virus while maintaining intact virus assemblies (15). For example, exposure of HAdV-2 to both free chlorine (20) and UV light (21) inhibited steps between attachment to the host cell and early protein RNA synthesis, most of which involving motifs of the three external capsid proteins (fiber, penton base, and hexon). Therefore, we hypothesize that, by using positive selection of aptamers that can bind infectious viruses with unmodified surface residues and counter selection to remove sequences that can bind disinfected viruses that have modified surface residues, we will

Science Advances Manuscript Template Page 3 of 23

be able to obtain a highly selective aptamer that can distinguish functional differences of whether the virus is infectious or not. In order to characterize the functional state of the virus and the concentration of HAdV that are infectious, plaque assay was used. This is the only method that can differentiate infectious from non-infectious virus, as opposed to methods based on nucleic acid detection, such us qPCR(11, 22), and, thus, is the assay that is used in this work to benchmark our results.

To monitor the selection progress, we used the qPCR technique to measure both the elution yield, defined as the amount of ssDNA bound to infectious HAdV divided by the total amount of added ssDNA (Fig. S1A); and the shift in melting curves after qPCR to assess sequence diversity of the DNA pools (23) (Fig. S1B). We then used high-throughput sequencing (HTS) to analyze the sequences from several selection rounds, allowing us to track the evolution of individual sequences over multiple selections rounds, and to identify "winner" aptamer sequences that are enriched with subsequent rounds, using the FASTAptamer analysis toolkit (24, 25). From this analysis, we identified a sequence, named HAdV-Seq4, that has been enriched over consecutive selection rounds (Fig. S1C) and predicted its secondary structure using UNAFold (Fig. S1D).

To characterize the binding affinity of HAdV-Seq4 to the virus target, we used both enzyme-linked oligonucleotide assay (ELONA) to obtain a dissociation constant (K_d) of (0.9±0.1) nM (Fig. 1B), which is at least one order of magnitude stronger than K_d 's of previously reported aptamers for other viral particles (26–28); and thermofluorimetric analysis (TFA) (29, 30) to obtain a K_d of (3.6 ± 0.6) x 10⁴ pfu/mL (Fig. S2A, purple). For both assays, noninfectious HAdV gave a much lower signal (Fig. 1B, Fig. S2B). The above results strongly suggest that the HAdV-Seq4 aptamer has a remarkably high affinity and selectivity for infectious HAdV over noninfectious HAdV.

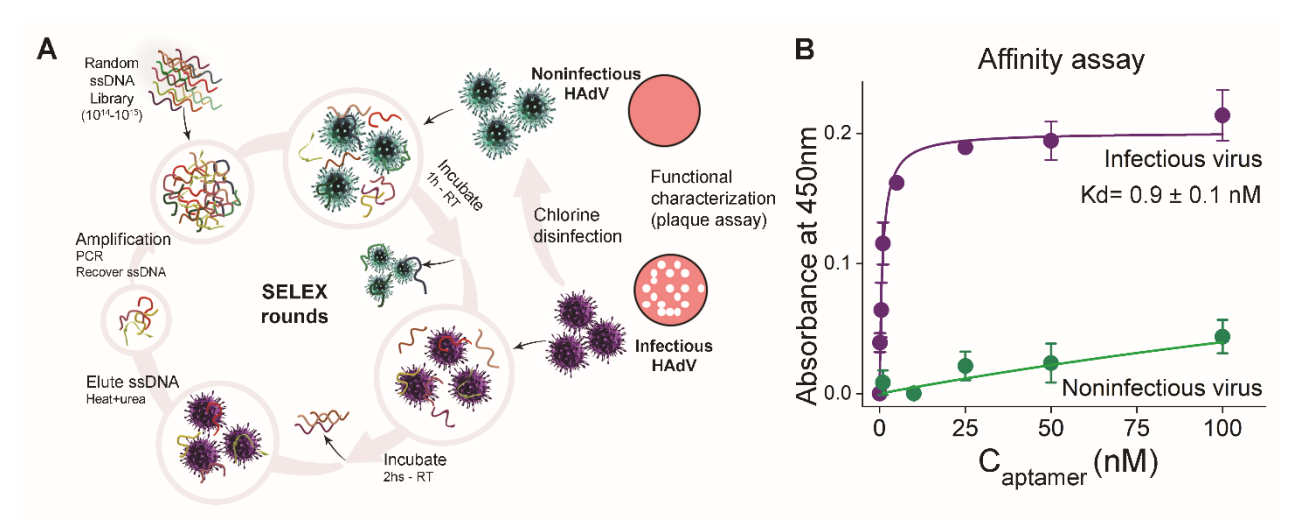


Fig. 1. *In vitro* **selection of infectious adenovirus-specific aptamer.** (A) Schematic representation of the *in vitro* selection process for HAdV. Positive and counter selections steps were added in each round to reach high specificity toward infectious virus. (B) Binding curves obtained from the ELONA assay. The dissociation constant (K_d) of the HAdV-Seq4 aptamer for infectious HAdV (0.9 nM) is more than 100 times higher than for noninfectious HAdV. n = 3 technical replicates (mean \pm SD).

To meet the ultrahigh sensitivity required for virus detection, we integrated the aptamers into solid-state nanopores (31, 32). Recognition elements, such as synthetic peptides, have previously been incorporated into nanopores to gain selectivity (33). However, with the pulsing-resistive approach used in these studies, the current signature detected still requires complex

Science Advances Manuscript Template Page 4 of 23

analysis to reach analyte selectivity. In contrast, single asymmetric nanochannel sensors in polymeric thick membranes can be characterized through steady-state current-voltage (I-V) measurements by sweeping the transmembrane potential at low frequencies (<0.1 Hz). This method significantly simplifies the signal detection and allows for direct detection of binding events that occur in sensing elements upon target recognition (31, 34), resulting in remarkable signal amplification capacity, as have been demonstrated for protein, DNA (35, 36) and small molecule detection (37). Moreover, the steady-state I-V curves contain precise information that is essential for quantification, background subtraction, and identification of potential interfering species.

175

176

177

178

179

180

181 182

183

184

185

186

187

188

189

190

191

192

193

194

195

196

197 198

199

200201

202

203204

205

206207

208

209

210

211

212

213

214

215

216217

218

219220

221

222

223

224

Therefore, to construct a highly sensitive sensor, we fabricated single nanochannel membranes by irradiation of polyethylene teraphthalate (PET) films with single swift heavy ions, and subsequent chemical etching of the generated single ion track. During the chemical etching process, both shape and size of the nanopore were adjusted to obtain a single bullet-shaped nanopore with dimensions less than 55nm in the narrow entrance (tip) and several hundreds of nm in the opposite entrance (base) (38, 39). A smaller tip size is necessary to enhance the sensitivity of the system, *i.e.* to enhance the variation in current signal when the virus binds to the pore. The HAdV-Seq4 aptamer was immobilized onto the inner wall of the nanopore after etching by EDC/Sulfo-NHS coupling between the carboxylate groups present on the surface of the nanopore after etching and the NH₂-modified HAdV-Seq4 aptamer (Fig. 2A, Fig. S3)(40). To prevent the nanopore surface from interfering with the aptamer binding to its target, a spacer was added between the amine group and the aptamer (Fig. S3B) The above modification procedure was verified by the current-voltage (I–V) measurements, showing a decrease in the current after grafting the aptamer onto the nanopore (Fig. S3A), due to a decrease in the effective nanochannel cross section due to the presence of the DNA.

We first determined the sensitivity of the aptamer-nanopore system for detecting HAdV by evaluating the ion transport property changes as a function of the HAdV concentrations (Fig. S4). The virus samples were incorporated to the reservoir facing the base of the nanopore (900 \pm 100 nm) and incubated for 30 min with the aptamer-nanopore system, followed by washing once with water to remove the excess of virus and then measuring the I-V characteristic curve in a KCl 0.1M solution (scheme in Fig 2B). We applied the virus samples to the reservoir facing the base of the nanopore to allow the virus to enter the nanopore and bind to the aptamer that is coated on the inside of the pore (Fig S5). We propose that the capture of the virus inside the nanopore produces a strong confinement, as the nanopore is ten times larger than the virus, resulting in a consequent signal amplification. The rectification efficiencies (free) were normalized by dividing each free from the samples containing viruses by the f_{rec} of the same system in the presence of just buffer ($f_{rec,0}$), to account for slight differences in the I-V curves characteristic for each nanopore after etching. Figure 2C shows the normalized rectification efficiency (freenorm) versus the concentration of virus. No significant change in the freenorm was observed after incubation with the infectious HAdV when the nanopore was not functionalized with the aptamer (Fig. 2C, black). Once the aptamer was grafted on the inner wall of the nanopore, the freenorm decreased with increasing amount of the infectious HAdV (Fig. 2C, purple), due to a change in the effective pore size with the virus incorporation, and thus in the ion transport properties. We have quantified the infectious HAdV concentration using plaque assays and benchmarked our results with this gold standard method to quantify infectious virus, since simpler and more recently developed methods like qPCR and immunoassays fail to determine infectivity status of the viruses (11) (Supplementary text 1). We were able to quantify the infectious HAdV in a broad range, from 6 pfu/mL to 6x10⁴ pfu/mL (Fig. S6A), with the ability to detect the HAdV down to 1 pfu/mL (Fig. S6B, Supplementary text 2). At such a low level of detection, the diffusion of the viral particles into the nanopore can be rate limiting. To determine the contribution of mass transport on our nanopore signal experiments, magnetic stirring was incorporated during the virus incubation step (Fig. S7). We found that the transport of virus to the nanopores is limiting the nanopore signal only for concentrations lower

Science Advances Manuscript Template Page 5 of 23

than 20 pfu/mL. However, incubation for thirty minutes was sufficient to obtain enough signal for detection, due to the high sensitivity of the nanopore.

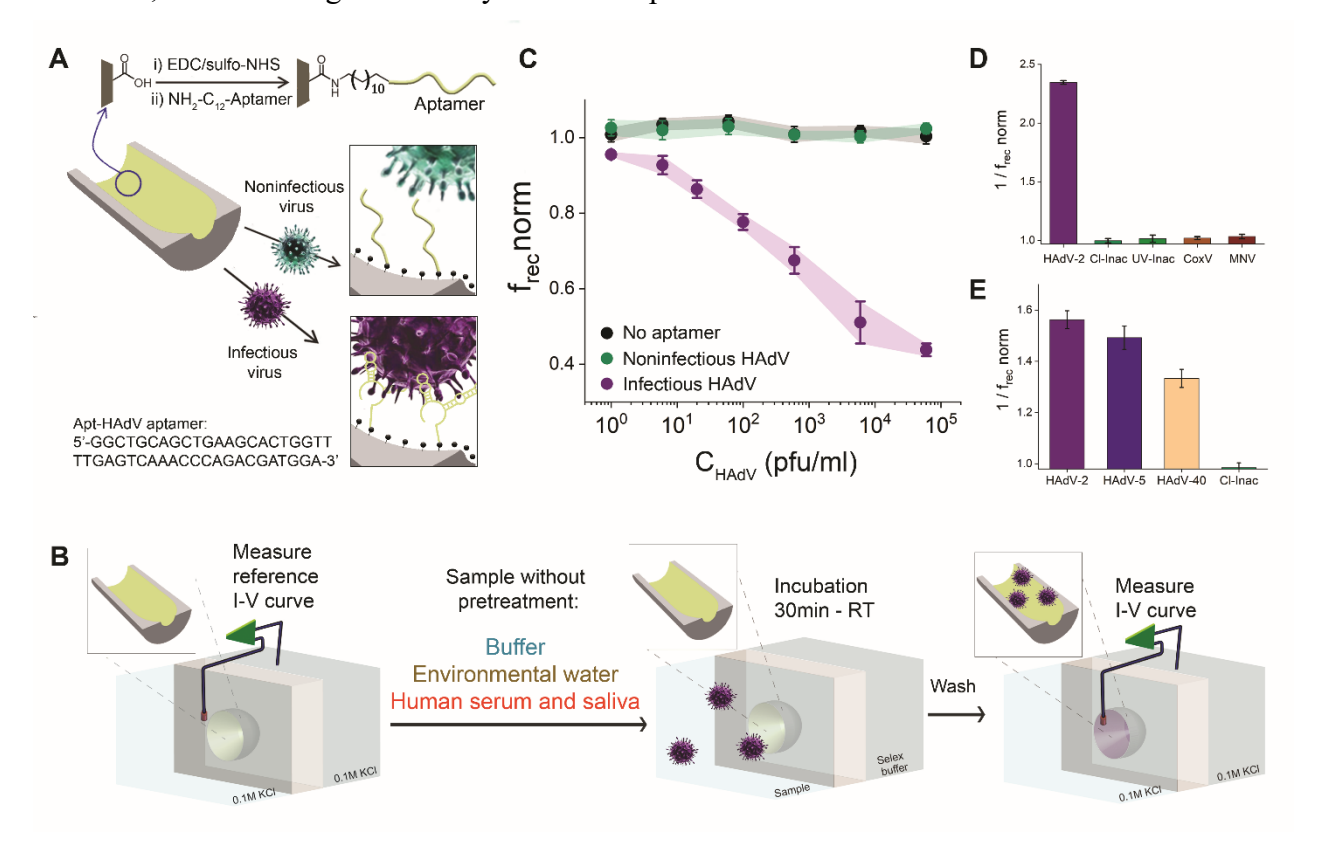


Fig. 2. Infectious HAdV detection using aptamer-functionalized nanopore sensors. (A) Scheme depicting the modification of the nanopore and the interaction of the aptamer with infectious HAdV samples. (B) Scheme of infectious HAdV detection by the aptamer-nanopore system. (C) Normalized rectification efficiencies (f_{rec}norm) versus virus concentration. n=3, technical replicates (mean ± SD). When no aptamer was added on the nanopore (black), no change in the f_{rec}norm was observed for infectious HAdV. Colors correspond to the nanopore modified with NH₂-C₁₂-aptamer for different concentrations of noninfectious virus (green) and infectious virus (purple). (D) Selectivity assay. Inverse of the f_{rec}norm obtained for infectious HAdV (HAdV-2), two noninfectious HAdVs using different inactivation mechanisms: free chlorine (Clinact) and UV-light (UV-inact), and two other viruses: Coxsackievirus B5 (CoxV) and Murine Norovirus (MNV). The concentration of each virus is 5x10⁴ pfu/mL. (E) Inverse of the f_{rec}norm obtained for different serotypes of infectious adenovirus (HAdV-2, HAdV-5 and HAdV-40) and comparison with an inactivated-HAdV sample at the same concentration (1x10³ pfu/mL).

To demonstrate the selectivity of our aptamer-nanopore sensor, we measured the rectification current in the presence of only noninfectious HAdV and other viruses. No significant change in the freenorm was observed in the presence of a wide range of concentrations of noninfectious HAdV (Fig. 2D) after incubated them for 30min, indicating high selectivity against noninfectious HAdV. Moreover, the sensor also shows remarkable selectivity against ultraviolet light-inactivated HAdV-2 (UV-inact), as well as against high concentrations of other waterborne viruses: Coxsackievirus B5 (CoxV) and Murine Norovirus (MNV) (Fig. 2D). In addition, we tested the sensor with different infectious HAdV serotypes, such as HAdV-2, HAdV-5, and HAdV-40 (Fig. 2E). Although the HAdV-Seq4 aptamer was selected against HAdV-2, it can recognize all three different serotypes of infectious adenoviruses tested. Among the serotypes, HAdV-40 is a type of HAdV that cannot replicate well in cell culture systems and thus is not as readily detectable

by a standard plaque assay. The fact that aptamer is able to detect other infectious HAdV serotypes supports that they may share a common structural motif that the aptamer can recognize, making it possible for our aptamer to detect many infectious HAdV serotypes, even if we select the aptamer to bind only one type. As a result, our method cannot differentiate virus subtypes in mixed samples. On the other hand, the signal obtained at the same concentration of virus is not always the same; it is particularly interesting to notice that the signal change for HAdV-2 and HAdV-5 are similar while for HAdV-40 is lower. This difference may correlate with slight differences in affinity as the aptamer was selected with the unique surface of HAdV-2. Overall, we successfully obtained a sensor that detect various infectious serotypes of adenoviruses, but not those that have been inactivated by disinfection methods.

Furthermore, we found that the sensor could quantify infectious HAdV in a mixture of infectious and non-infectious HAdV (Fig. S8) and showed a high degree of correlation with a plaque assay as a benchmark (Fig. 3A). The ability of our sensor to quantify infectious HAdV in real environmental samples was also tested with various types of samples, including drinking water samples from tap water in Champaign (IL, US), drinking water samples from a borehole in a secondary school in Uganda (Africa), and wastewater effluent samples (IL, US). The three samples were measured using the sensor without any pretreatment of the water (Fig. S9) and the results were compared with the plaque assay results (Fig. 3B). For both drinking water samples, the recovery yield was $(102.5 \pm 5.5)\%$, while for the wastewater effluent the recovery yield was $(95 \pm 7)\%$, indicating that our sensor can quantify infectious HAdV in real water samples despite the presence of potential interfering background substances. Furthermore, when a 99.9% inactivated HAdV was spiked into these water samples, it was possible to quantify 10 pfu/mL of infectious HAdV in the presence of $7x10^3$ pfu/mL total HAdV, in all cases (Fig. S10). Overall, these results demonstrate that the performance of the aptamer-nanopore sensor is largely unaffected by the complex matrices of the real water samples.

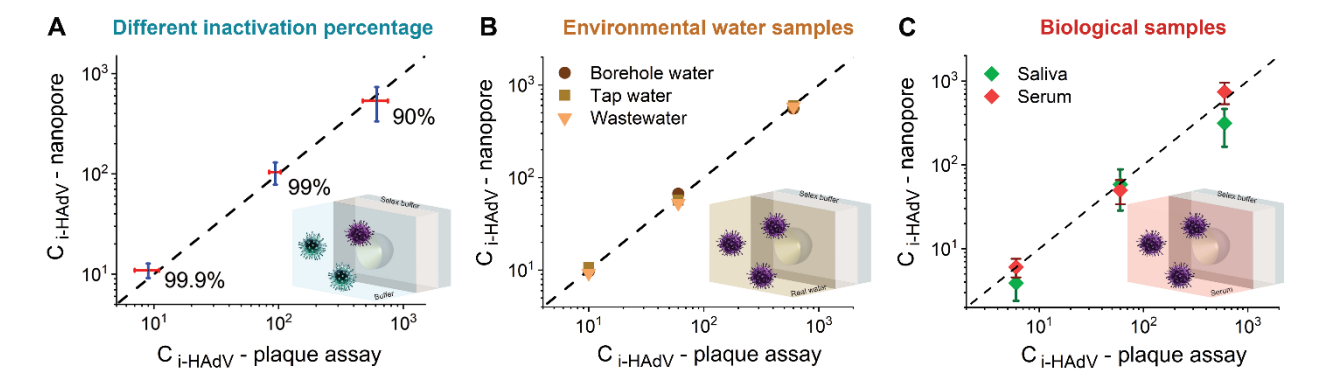


Fig. 3. Direct quantification of infectious HAdV in real samples with the aptamer-nanopore system. (A) Quantification of infectious HAdV in a mixture of infectious and noninfectious HAdV by comparison of aptamer-nanopore sensor (y-axis) with plaque assay (x-axis). (B) Quantification of infectious HAdV in different real water samples without any pretreatment or dilution by comparison of aptamer-nanopore sensor (y-axis) with plaque assay (x-axis). (C) Quantification of infectious HAdV in human serum and saliva without dilution of the biological sample by comparison of aptamer-nanopore sensor (y-axis) with plaque assay (x-axis). n=3, technical replicates (mean \pm SD).

To extend this aptamer-nanopore sensor for rapid diagnostics of infectious HAdV directly from bodily fluids, we spiked 1.5ml of human serum and saliva with 15ul of infectious HAdV solution of different concentrations; therefore, avoiding significant dilution of the biological sample. We observed a decrease in the freenorm with different concentrations of infectious HAdV

(Fig. S11), and their performance was similar to those measured in buffer (Fig. 3C). In our approach, the signals from interfering species in human serum and saliva samples can be removed readily by a washing step to remove those species that do not bind to the aptamer and by measuring the I-V curve in the sample without virus and normalizing the frec to obtain the frecnorm signal. These results demonstrated the advantage of obtaining the precise information that the I-V curve contains, that is essential not only for quantification but also for a simple background subtraction and removal of potential interferences, that is not possible with other nanopore methods. However, we cannot rule out the possibility of the geometry of the nanopore itself contributing as well to the results in real samples.

292

293

294

295

296297

298299

300

301

302

303304

305

306

307

308

309

310

311

312313

314

315

316

317

318

319

320

321

322

323324

325

326

327328

329

330

331

332

333334

335

336

337

338

339

340

Since our selection method does not depend on known biomarkers to differentiate infectious and non-infectious viruses, it can be readily applied to newly emerging viruses, which have been appearing worldwide at an increasing rate, without any information about the inactivation mechanism. To demonstrate the generality of our method, we applied our sensor to detect SARS-CoV-2, the newly emerged coronavirus responsible for the COVID-19 pandemic, which has infected nearly 120 million people and resulted in more than 2.3 million deaths worldwide as of late-February 2021. To retain the advantages of applying a whole-virus *in-vitro* selection approach in applying our sensor to SARS-CoV-2, which is classified as a Biosafety Level 3 (BSL-3) agent, *in-vitro* selection was performed using a pseudotyped SARS-CoV-2 virus. The pseudotyped virus is generated from a lentivirus (HIV) that displays the SARS-CoV-2 spike (S) protein within the viral envelope, and thus closely mimics the surface and entry mechanism of SARS-CoV-2 but are defective in continuous viral replication (41, 42) (Supplementary text 3). Since our SELEX strategy to differentiate infectious from noninfectious viruses depends only on the surface of the viruses, using this pseudotyped virus allowed us to work in a BSL-2 lab. Because of their advantage at modelling the SARS-CoV-2 surface and entry mechanisms requiring only a BSL-2 laboratory, pseudotyped SARS-CoV-2 have been used previously to study the cell type susceptibility, virus receptor, entry pathway, and protease priming for SARS-CoV-2, and also to identify several potential drug targets and neutralizing antibodies for SARS-CoV-2 (43). Thus, pseudotyped SARS-CoV-2 has been widely used as a reliable and robust model for infectivity.

To achieve high selectivity against active SARS-CoV-2 over inactive SARS-CoV-2, we performed counter selection against UV-light inactivated pseudotyped SARS-CoV-2 (Fig. S12). UV-inactivation produces damage in the genome and in the proteins on the surface of the virus, while largely maintaining the intact virus structure. Furthermore, to obtain an aptamer with the ability to distinguish against other viruses, including very similar coronaviruses, we incorporated counter-selection against a lentivirus pseudotyped with SARS-CoV-1 S protein and a lentivirus pseudotyped with influenza hemagglutinin 5 and neuraminidase 1 proteins (H5N1). Ten rounds of selection were performed (Fig. S13). After sequencing different rounds with HTS, we identified a sequence, named SARS2-AR10, that showed good enrichment over subsequent selection rounds (Fig. S13C). ELONA results showed a K_d of (79±28) nM with high selectivity against UVinactivated pseudotyped SARS-CoV-2 (Fig. S14), and Microscale Thermophoresis (MST) also showed that SARS2-AR10 binds to active SARS-CoV-2 but not to UV-inactivated pseudotyped SARS-CoV-2 or other viruses like 229E coronavirus, pseudotyped SARS-CoV-1, or pseudotyped influenza H5N1 (Fig. S15), demonstrating the high selectivity of SARS2-AR10 toward active SARS-CoV-2. For COVID-19 diagnostic, it is important to differentiate between different coronaviruses; thus, strict counter selection steps were applied to tune the selectivity of the SARS2-AR10 aptamer

To gain insights into SARS2-AR10 selectivity, we assessed the binding of our aptamer to isolated SARS-CoV-2 S1 protein in solution with and without UV-treatment using ELONA assay the binding curve. Fig. S16 shows that SARS2-AR10 binds to the active S1 domain with a lower affinity than toward pseudotyped SARS-CoV-2. This is an expected result since the aptamer was

Science Advances Manuscript Template Page 8 of 23

selected using the pseudovirus, which mimics SARS-CoV-2 spike protein in its native conformation, and thus it likely binds better to the accessible surface residues of spike protein of SARS-COV-2, not those embedded within the envelope proteins in the pseudovirus. In addition, since the trimeric spike protein assembles on the surface of the virus in trimers, our aptamers likely bind these spike proteins, but not individual spike protein. Furthermore, the affinity of the aptamer toward the UV-inactivated S1 protein is lower. These results suggest that the specificity is mainly achieved through protein recognition and inactivating modifications.

We then determined the ability of the SARS2-AR10-nanopore system to detect and quantify SARS-CoV-2 with different concentrations of active pseudotyped SARS-CoV-2 after 30 min and 2 hr virus incubation (Fig. S17). An increase in the virus incubation time resulted in a higher sensitivity and lower detection limit. With 2 hr incubation, the sensor detected as low as 1x10⁴ copies/mL and quantified a broad range of virus concentrations, from 1x10⁴ copies/mL to 1x10⁸ copies/mL (Fig 4A). Thus our method can reach the lowest detectable concentrations in individuals that have tested positive for SARS-CoV-2 in saliva and nasal swabs (1). Furthermore, the lowest detectable concentration of our method (1x10⁴ copies/mL) is similar to the detection limit reached by RT-PCR (3x10³ copies/mL) (44) and other nucleic acid detection methods, for instance those based on LAMP reaction (5x10⁴ copies/mL) (2, 45). We further tested the selectivity of our aptamer-nanopore sensor against inactive SARS-CoV-2 (Fig 4A) and against an endemic coronavirus that produces the common cold, 229E coronavirus, as well as pseudotyped SARS-CoV-1 and H5N1 influenza virus (Fig. 4B) and found no significant change, supporting the high selectivity of our sensor for active SARS-CoV-2 against inactive SARS-CoV-2, other coronaviruses, and influenza virus.

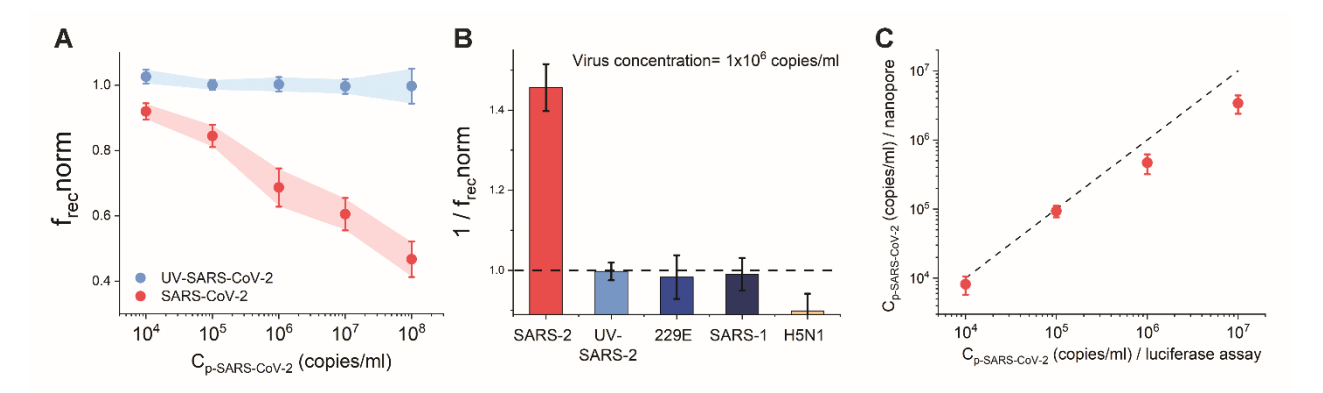


Fig. 4. Quantification of active pseudotyped SARS-CoV-2 with the aptamer-nanopore system. (A) Normalized rectification efficiencies versus virus concentration. n=3, technical replicates. Colors correspond to the nanopore modified with different concentrations of UV-inactivated pseudotyped SARS-CoV-2 (blue) and active pseudotyped SARS-CoV-2 (red) (B) Selectivity assay. Inverse of the f_{rec} norm obtained for active pseudotyped SARS-CoV-2 (SARS-2), UV-inactivated pseudotyped SARS-CoV-2 samples (UV-SARS-2); another coronavirus: 229E, and two other pseudoviruses: SARS-CoV-1 (SARS-1) and influenza virus (H5N1). The concentration of each virus is 1×10^6 copies/mL. (C) Comparison of aptamer-nanopore sensor (y-axis) with luciferase assay (x-axis) to quantify active pseudotyped SARS-CoV-2 in human saliva without dilution of the biological sample. n=3, technical replicates (mean \pm SD). Each of these measurements was performed with a new membrane.

Finally, we spiked 12 human saliva samples with different concentrations of active pseudotyped SARS-CoV-2 and observed a decrease in the f_{rec} norm with different concentrations of active SARS-CoV-2 (Fig. S18). The results show a good correlation between the concentration calculated using the obtained f_{rec} norm in saliva compared with the concentration measured with

Science Advances Manuscript Template Page 9 of 23

luciferase assay (Fig 4C), indicating that our aptamer-nanopore system can quantify pseudotyped SARS-CoV-2 in saliva without any pretreatment of the biological sample. When we immobilized a control sequences in the nanopore and we repeat the experiment under the same conditions with a high concentration (1x10⁷copies/mL) of spiked pseudotyped SARS-CoV-2 in saliva, we observed no significant change in the nanopore signal (Fig. S19). Therefore, the changes in the freenorm are related to the specific binding of the SARS-CoV-2 to the aptamer.

Discussion

The sensitivity of our method rivals those for standard viral assay methods such as the plaque assay and qPCR with the major advantage being that it is much faster (30 min to 2 hours), as we do not need to wait for plaques to fully develop (e.g., 10 days for HAdV) or the genome to be extracted and replicate (e.g., 24 hours for HAdV). In addition, our method can detect infectious viruses that cannot replicate well in cell culture systems, such as HAdV-40, and thus are not readily detectable by the standard plaque assay. The sensitivity enhancement and low LOD obtained with the aptamernanopore may be related to two main factors. First, viruses are known to present multiple antigens (e.g., S protein for SARS-CoV-2) on the surface and thus multiple identical binding sites for the aptamers. Thus these multivalent binding avidity can increase the sensitivity, as reported previously (46). In addition, it has been demonstrated that the presence of charged groups on the nanopore walls, such as DNA aptamers, can lead to strong ionic preconcentration effects inside the nanopore. Such a nanoconfinement effect is also known to increase the sensitivity (47, 48).

In comparison to qPCR or other nucleic acid detection-based tests, our system can detect intact viruses directly in real samples, without the need to collect and disrupt the viruses for nucleic acid extraction, thereby resulting in high selectivity against noninfectious virus. Additionally, these simpler and more recently developed methods based on nucleic acid detection cannot inform virus infectivity and thus, in this work, the only gold standard method available to benchmark our aptamer-nanopore sensor was the plaque assay.

We choose free chlorine as the disinfection method for HAdV-2 in water, because it is the most common disinfection method for treatment of water samples. To demonstrate that the same method of SELEX can be applied to other disinfection methods, we further showed that our method could also distinguish active from UV-inactivated SARS-CoV-2 pseudovirus, suggesting that we can achieve selectivity regardless which of these two procedures are used for inactivation. Furthermore, since our aptamer can differentiate infectious from noninfectious viruses, a detailed characterization of the binding targets of our aptamers can also be applied to reveal surface changes responsible for the loss of infectivity for each of the inactivation treatment.

We were able to successfully apply the aptamer-nanopore system to two different type of viruses, showing the broad application range of our approach. On one hand, the HAdV is a non-enveloped virus, with a protein capsid as the surface, which makes it more rigid and probably with a compact surface charge; while SARS-CoV-2 is an enveloped virus, where the surface consists of a more flexible lipid bilayer in which surface proteins are embedded. These surface differences can affect the nanopore response, which is highly dependent on the charge and size of the target. These viruses' differences as well as differences in the binding affinities of the aptamers, where the HAdV-Seq4 has 80 times stronger affinity than SARS2-AR10, can explain the different responses in terms of virus incubation time and analytical performance. Thus, further optimization of the aptamer sequence could help to decrease the incubation time needed to reach the same sensitivity and detection limit for SARS2-AR10 as for HAdV-Seq4. Additionally, since several aptamers for the spike protein, S1 domain or RBD of the spike protein of SARS-CoV-2 have been reported (49–51) since our work has begun, immobilizing these aptamers into the nanopore will further enhance LoD and sensitivity.

Science Advances Manuscript Template Page 10 of 23

Furthermore, our SELEX strategy to differentiate infectious from noninfectious viruses depends only on the surface of the viruses, thus aptamer selection can proceed on pseudotyped viruses, lessening the need of working with new emerging pathogens that are classified as BSL-3 with very restricted worldwide availability for whole virus experiments. We propose that our workflow for aptamer selection against SARS-CoV-2 using a pseudotyped virus that can mimic the native state of the surface proteins may well be applicable as a whole virus selection strategy for other emerging pathogens.

These results demonstrate the enormous design flexibility offered by our aptamer-nanopore sensors. The implementation of SELEX to obtain specific aptamers for infectious viruses, and their subsequent assembly into the corresponding aptamer-nanopore systems, where the steady-state I-V curves contain precise information that allows quantification and background subtraction, make it possible to quantify viruses in samples ranging from complex environmental samples to untreated biological fluids, which will allow a wide range of applications for rapid and selective detection of both current and emerging viral pathogens around the world.

Materials and Methods

DNA library

All the DNA sequences were purchased as synthetic oligonucleotides from Integrated DNA Technologies (IDT). A random ssDNA library (1nmol) and reverse and forward primers were purified by polyacrylamide gel electrophoresis (PAGE).

The ssDNA pool consisted of a central random region of 45 nucleotides flanked by two constant sequences at the 3' and 5' ends that act as primer regions for amplification (See Table 1). The reverse primer was modified with biotin to separate ssDNA from amplified double stranded PCR products using streptavidin-coated beads during the *in-vitro* selection process. Unmodified FwdP and RevP were used for PCR amplification after the final round of the *in vitro* selection, for HTS libraries preparation, and for qPCR quantification.

Proper folding of ssDNA library and pools was attained by denaturing at 95°C for 10 minutes, followed by cooling on ice for 10 min before use in each round.

Table 1. DNA sequences used in this work.

Name	DNA sequence (5' to 3') / In bold IDT	
	modification	
DNA library HAdV	GTCCATCGTTCGGTAGTG-45N-	
J	GGCTAACTGTCCACGATT	
Forward primer (FwdP) HAdV	GTCCATCGTTCGGTAGTG	
Reverse primer (RevP) HAdV	/5Biosg/AATCGTGGACAGTTAGCC	
T20	TTTTTTTTTTTTTTTTT	
HAdV-Seq4	GGCTGCAGCTGAAGCACTGGTTTTGAGTCAAAC	
1	CCAGACGATGGA	
3AmMO-Aptamer	GGCTGCAGCTGAAGCACTGGTTTTGAGTCAAAC	
1	CCAGACGATGGA /3AmMO/	
NH ₂ -C ₁₂ -HAdV-Seq4	/AmMC12/GGCTGCAGCTGAAGCACTGGTTTTG	
2 12 12 13 14	AGTCAAACCCAGACGATGGA	
DNA library SARS-CoV-2	ACCGTCAGTTACAATGCT – 45N -	
,	GGCTGGACTATCTGTGTA	

Science Advances Manuscript Template Page 11 of 23

Forward primer (FwdP) SARS-CoV-2	ACC GTC AGT TAC AAT GCT	
Reverse primer (RevP) SARS-CoV-2	/5Biosg/TAC ACA GAT AGT CCA GCC	
SARS2-AR10	CCCGACCAGCCACCATCAGCAACTCTTCCGCGTC CATCCCTGCTG	
NH ₂ -C ₁₂ -SARS2-AR10	/AmMC12/CCCGACCAGCCACCATCAGCAACTC TTCCGCGTCCATCCCTGCTG	

Human Adenovirus propagation and viability assessment

Human Adenovirus Serotype 2 (HAdV-2, VR-846) was propagated with A549 cells (CCL-185), both obtained from the American Type Culture Collection (Manassas, VA). Cell incubation, viral propagation, and viral infectivity assessment methods were similar to previously reported protocols (20). Briefly, A549 cell monolayers were maintained in flasks at 37°C with 5% CO₂ with modified Ham's F12K media + 10% fetal bovine serum + 0.25 $\mu g/mL$ amphotericin B + 100 units/mL penicillin + 10 $\mu g/mL$ streptomycin (Sigma-Aldrich, St. Louis, MO). To propagate the viruses, HAdV-2 liquid stock was inoculated onto A549 cell monolayers and incubated at 37°C with 5% CO₂ until cytopathic effects showed up. Viruses were released from the cells by freeze-thaw cycles. The lysates were centrifuged, and the supernatants were passed through 0.45 or 0.22 μm vacuum filters to remove large debris (Millipore, Billerica, MA). The filtrate was purified and concentrated using a 300 kDa ultrafiltration membrane (Millipore) in Amicon stirred cells. For some later batches of propagation, the filtrate was purified and concentrated using sucrose cushion ultracentrifugation. The concentrated virus stocks were in 1 mM carbonate buffer solution (CBS, Fisher Scientific) stored at -80°C.

The virus infectivity was assessed with soft agar-overlay plaque assay and plaque counting at 9 or 10 days post infection were used to determine virus titers.

Inactivation of HAdV - Chlorine treatment

The inactivation of HAdV-2 by free chlorine was previously described (15, 20). In brief, a batch reactor with 1 mM CBS under continuous magnetic stirring was spiked with HAdV-2. The temperature was maintained constant with a water bath, and pH was adjusted with hydraulic acid or sodium hydroxide solution. An initial sample was taken to measure initial viral concentration with the plaque assay method, and then sodium hypochlorite solution was added into the reactor while a timer was started at the same time. Samples were taken along with time and immediately mixed with 0.1% sodium thiosulfate to quench the chlorine and stop the inactivation process. The time points at which samples were added into sodium thiosulfate were recorded. Although the initial sample had no chlorine, it was also mixed with 0.1% sodium thiosulfate so that all the samples are comparable. The chlorine concentration was monitored with the N,N-diethyl-p-phenylene diamine (DPD) method (52) and the sampling times and the chlorine concentrations were both recorded. Chlorine reacts extremely fast with viruses, leaving no time to measure the initial chlorine concentration in this reactor, so a second reactor controlling for the addition of virus stock was prepared in order to make the measurement of initial chlorine concentration possible.

The inactivated HAdV were dialyzed with 1mM CBS buffer to remove the excess of sodium hypochlorite and sodium thiosulfate. In this way, the infectious and noninfectious HAdV are in the same buffer for the *in vitro* selection process.

Inactivation of HAdV-2 by low pressure ultraviolet light

Science Advances Manuscript Template Page 12 of 23

The ultraviolet (UV) light inactivation experiments followed previously published methods except that a low-pressure UV lamp (GSL233T5L/SL, Atlantic Ultraviolet Corporation, Hauppauge, NY) was operated at 10 W and no bandpass filters were installed. A recirculating water-jacketed reactor (20°C) containing 1 mM CBS was spiked with HAdV-2 under continuous magnetic stirring. The fluence was calculated as the product of the average irradiance and exposure time and four factors were measured for necessary corrections based on the literature (53). The irradiance distribution across the irradiated water surface was measured with a 1400A radiometer and SEL 240 detector (International Light, Peabody, Massachusetts) in order to correct for the nonuniformity of the light distribution (petri factor). The UV absorbance at 254 nm of the water sample to be treated by UV was measured with UV2700 Shimadzu spectrophotometer to adjust for water depth since UV can be absorbed by water (water factor). Distance of suspension from the UV lamp (divergence factor) and water surface reflection (reflection factor) were also considered into the calculation. With the average irradiance obtained and the desired fluence, the required exposure time was obtained.

Other waterborne viruses

Other viruses tested in this study include Human Adenovirus Serotype 5 (HAdV-5), Human Adenovirus Serotype 40 (HAdV-40), Coxsackievirus B5, and Murine Norovirus. HAdV-5 (VR-5) was obtained from ATCC and its propagation method and viral infectivity assessment are the same as those described for HAdV-2. HAdV-40 (Ad40, Dugan strain, p.3, clone 6A) was obtained from Theresa Cromeans (54) (Centers for Disease Control and Prevention). Coxsackievirus B5 Faulkner (VR-185) was obtained from ATCC and passaged in buffalo green monkey kidney cell (QUIDEL, San Diego, CA) monolayers three times, and then purified and concentrated following the protocol of HAdV-2. Murine Norovirus was originally provided by Herbert Virgin (formerly at Washington University School of Medicine, St. Louis, MO) and propagated using RAW 264.7 cells (TIB-71) obtained from ATCC. The virus purification and concentration protocol were similar to those of HAdV-2.

Cell culture for pseudovirus production

293T embryonic kidney cells (ATCC# CRL-1573) and human hepatoma cell line Huh7 (obtained from Thomas Gallagher at Loyola University) were cultured in DMEM supplemented with 10% fetal bovine serum (Gibco), 100 units of penicillin, and 100 μg/mL streptomycin (Invitrogen).

Production and quantification of pseudotyped viruses

Pseudoviruses were created using the following plasmids: SARS-CoV-1 spike protein, SARS-CoV-2 spike protein, hemagglutinin (HA) and neuraminidase (NA) isolated from the highly pathogenic avian influenza virus A/Goose/Qinghai/59/05 (H5N1) strain, and the HIV-1 pro-viral vector pNL4-3.Luc.R-E- (obtained through the NIH AIDS Research and Reference Reagent Program). All pseudovirions were produced by transient co-transfection of 293T cells using a polyethyleneimine (PEI)-based transfection protocol. Five hours after transfection, cells were washed with phosphate-buffered saline (PBS), and 20 mL of fresh media was added to each 150 mm plate. Twenty-four hours post transfection, the supernatant was collected and filtered through a 0.45 μM pore size filter. Pseudotyped virus was concentrated by ultra- centrifugation. The pseudovirus was layered onto a 30% (wt/vol) sucrose cushion and centrifuged at 26,000 rpm for 2 hours in a ThermoFisher AH-629 rotor. The pelleted pseudovirus was resuspended in sterile PBS, aliquoted, and frozen for future use. The pseudovirus titer was determined using a quantitative p24 lentivirus ELISA kit (Takara Lenti-X p24 Rapid Titer Kit, cat#632200).

Science Advances Manuscript Template Page 13 of 23

UV-inactivation of pseudotyped SARS-CoV-2

We targeted 293T cells that were transfected with pcDNA3.1(+)-ACE2 and pCSDest-TMPRSS2 for 6 h. The cells were then trypsinized and seeded at 1x10⁵ cells/well in DMEM complete into white bottom 96-well plates (100 μL/well), then incubated for 16 hours at 37 °C and 5% CO₂. To evaluate the efficacy of UV irradiation of the SARS-CoV-2 pseudotyped virus, the pseudovirus was placed in an open plastic petri dish and positioned under the UV light source in a biosafety cabinet and irradiated at differing time points with 134 μW/cm². The UV treated pseudovirus containing a luciferase reporter gene was added to the 96-well plates along with non-UV treated pseudovirus as a control. Plates were incubated at 37 °C and 5% CO₂ for 48 hours and viral infection was determined by luminescence using the neolite reporter gene system (PerkinElmer). Data was normalized to non-UV treated pseudovirus (100% infectivity).

Production and Quantification of Infectious 229E-CoV.

229E-CoV was obtained as a gift from Tomas Gallagher (Loyola University). The virus was propagated in Huh-7 cells and stocks were frozen at -80 °C. For quantification, approximately 1x10⁶ Huh-7 cells/well were seeded in 6-well tissue culture plates (Corning) and allowed to grow to 90% confluence for 24 h. Viral stocks were serially diluted 10-fold (10⁻² – 10⁻⁸), culture media was removed, and replaced with 400 μL of each viral stock dilution in triplicate. Plates were incubated at 33 °C, 5% CO₂ for 2 hours, rocking gently every 20 min. After 2 hours, the virus was removed and replaced with 2 mL of a 1:1 mixture of 2X MEM media and 2.4% Acivel-591. Plates were incubated at 33 °C, 5% CO₂ for 96 hours. Plates were fixed with 10% formalin and stained with 1% crystal violet to visualize plaques.

Water samples and biological samples

- Tap water was obtained from the tap at the University of Illinois at Urbana-Champaign, in Illinois,
- 572 US. A more complex drinking water sample was obtained from a borehole at Panyodoli Secondary
- School in Kiryandongo District, Uganda. Wastewater secondary effluent was obtained from Urbana
 - & Champaign Sanitary District in Illinois, US.
- Human serum from human male AB plasma (USA origin, sterile-filtered) was purchased from
 - Sigma-Aldrich. Pooled human saliva samples were purchase from BioIVT

In-vitro selection of the virus-specific aptamers

- A schematic diagram of the *in vitro* selection process is shown in Fig. 1A.
- First round of in vitro selection: The heat denatured ssDNA library (1 nmol) was mixed with 50 μl of 6x10⁵ pfu/mL infectious virus in a total volume of 350 μL of SELEX buffer (20 mM TRIS, 100 mM NaCl and 2.5 mM MgCl₂, pH 7.2) and incubated for 2hr at room temperature. Then, the unbound sequences were removed using an Amicon Ultra-0.5 100 kD filter, followed washing 4 times with 400 µL of SELEX buffer to ensure removal of all unbound sequences. To elute the bound sequences, we heated the filter countaining the virus and bound sequences for 15 min at 95 °C in the presence of 8 M urea and then centrifuged, collecting the fraction that flowed through the filter in a new tube. Then, to concentrate and desalt the DNA, we used an Amicon Ultra-0.5 10 kD filter and washed 2 times with SELEX buffer (300 µL each time). We took 1 µL of the eluted ssDNA to quantify the amount of DNA by qPCR, and the remaining pool was used as a template for

Science Advances Manuscript Template Page 14 of 23

amplification of bound sequences by PCR (30 cycles of 1 min at 95 °C, 30 s at 52 °C, 1 min at 72

- 591 °C, followed by 10 min at 72 °C) to obtain the dsDNA pool. The PCR was carried out in a total
- volume of 50 µL with the reverse primer labelled with a biotin, using a GoTaq Flexi DNA 592
- Polymerase (Promega). Finally, ssDNA was recovered by streptavidin-coated magnetic beads. We 593
- took 1 µL of the recovered ssDNA to quantify the amount of DNA by qPCR and the remaining 594
- DNA was used for the following round. 595
- 2nd to 11th round of in vitro selection: Enriched pools (200 pmol) were heat denatured as described 596
- before and mixed with 25 µL of 1x10⁵ pfu/mL noninfectious virus in a total volume of 100 µL of 597
 - SELEX buffer as the counter selection step. After incubation for 1 hr at room temperature, the
- unbound sequences were recovered using an Amicon Ultra-0.5 100 kD cutoff and washed 2 times 599
- with 100 µL of SELEX buffer. We collected the unbound sequences that flowed through the filter 600
 - and incubated them with 50 μ L of $6x10^5$ pfu/mL infectious virus in a total volume of 350 μ L as the
- positive selection step. From here the protocol is the same as for round 1 for sequence elution, 602
- 603 desalting, and PCR amplification.
- All Amicon Ultra-0.5 filters were treated with 1 mM of T20 for 30 min to avoid nonspecific 604
- adsorption of the library and pool sequences on the filter, followed by washing for 3 times with 605
- SELEX buffer. 606
- A new PCR using unlabeled primers was performed to prepare the pools for high-throughput 607
- 608 sequencing.

598

601

611

618 619

631

632

- The in-vitro selection process to obtain an aptamer specific for infectious SARS-CoV-2 was 609
- performed using the same procedure as for HAdV, with the following changes. In this case, 1x10⁸ 610
 - copies/mL pseudotyped SARS-CoV-2 was used in the positive selection rounds, while UV-
- inactivated pseudotyped SARS-CoV-2, pseudotyped SARS-CoV-1 and pseudotyped H5N1 were 612
- used for counter selection steps $(5x10^9 \text{ copies/mL of each})$. The SELEX buffer was 1X PBS, with 613
- 2.5 mM MgCl₂, 0.5 mM CaCl₂, pH 7.4. To increase the yield from the pool elution step from the 614
- 100kD filter, instead of eluting in 8 M urea, elution was performed in the SELEX buffer, at 95 °C 615
- for 10 min. This allowed us to directly use this eluted sample without concentration/desalting with 616
- 617 the 10kDa filter.

In vitro selection monitoring

- qPCR was used to monitor the SELEX process in two ways: (1) testing the enrichment of the pools 620
- (elution yield) using an absolute quantification, and (2) assessing sequence diversity of the pools 621
- (convergence of the aptamer species) by monitoring the melting curve (23). 622
- Real-time PCR experiments were conducted with a CFX96 Real-Time PCR System (BioRad) 623
- according to the manufacturer's instructions. All reactions were performed in 10 µL reaction 624
- volumes in 96-well plates for PCR. A standard qPCR mixture contained 5 µL SsoFast EvaGreen 625
- Supermix (BioRad), 0.3 μL of 500 nM of each unlabeled primer, 3.4 μL of H₂O and 1 μL DNA 626
- template. Thermal cycling consisted of an initial denaturation at 98 °C for 2 min followed by 40 627
- cycles of denaturation at 98 °C for 5 s and annealing and extension at 52 °C for 10 s. After these
- 628 amplification cycles, the melting curve analysis was performed from 65 °C to 95 °C. Threshold 629
- cycle (Ct) values were determined by automated threshold analysis. 630

High-throughput sequencing of selection rounds

- Selected selection cycles (rounds 4, 6, 7, 8, 9, 10, and 11 for HAdV selection and rounds 3, 5, 7, 8, 633
- and 9 for SARS-CoV-2 selection) were prepared for high-throughput sequencing (HTS) analysis 634
- on an Illumina HiSeq4000 platform (performed by the DNA Services Lab of the Roy J. Carver 635
- 636 Biotechnology Center at UIUC), using the Celero DNA Seq kit (Nugen/Tecan) for library
- preparation. Briefly, library preparation involved first performing end repair of fragmented DNA, 637

Science Advances Page 15 of 23 Manuscript Template

followed by adaptor ligation, and PCR amplification to produce the final libraries. This kit incorporated different unique dual indexes that allowed the sample analysis of all rounds on one lane. After purification of the PCR product with Agencourt® AMPure XP Beads (Beckman Coulter), quantification of the DNA was carried out using a fluorescence method (Qubit kit – dsDNA Broad Range), and approximately equal amounts of each library containing specific indexes were mixed. After a quality control (qPCR quantification and fragment analyzer of the DNA, performed by the DNA Services Lab), 100 bp single end sequencing was carried out.

After demultiplexing, HTS data was analyzed using the FASTAptamer software (24). FASTAptamer-Count allows us to count the number of times each sequence is sampled from a population and then rank and sort the sequences by abundance, while FASTAptamer-Enrich was used to calculate fold-enrichment for each sequence present in more than one round of the selection by comparing the RPM of the sequence from one population by the RPM in another.

Binding affinity tests

Enzyme-linked oligonucleotide assay (ELONA)

ELONA was used to determine the binding affinity of the HAdV-Seq4 aptamer toward HAdV and the SARS2-AR10 aptamer to pseudotyped SARS-CoV-2. Infectious HAdV (6x10⁵ pfu/mL) or active pseudotyped SARS-CoV-2 (5x10⁸ copies/mL) was coated on a microplate at room temperature for 2 hr. After blocking with 100 μL of 5% bovine serum albumin (BSA) in phosphate-buffered saline for 1 h at room temperature, the biotin-labeled aptamer was added to the individual wells at various concentrations (0.1 to 1000 nM) in the SELEX binding buffer and incubated for 1 h at room temperature. Horseradish peroxidase-conjugated streptavidin (1:500) was added and incubated for 45 min. Color development was achieved by adding tetramethylbenzidine chromogen substrate (TMB). After adding 2 M H₂SO₄ as stop solution, the optical density at 450 nm (OD450) was determined using a microplate reader. The same procedure was done for the free chlorine inactivated HAdV and UV-inactivated pseudotyped SARS-CoV-2.

For ELONA assay using the S1 protein, the same procedure was repeated but the microplate was coated with SARS-CoV-2 Spike protein S1 (Invitrogen aa11-682).

Thermofluorimetric Analysis (TFA)

Thermofluorimetric analysis (TFA) measures the fluorescence of a mixture of DNA and intercalating dye as a function of temperature (29, 30). Intercalating dyes are only highly fluorescent when bound to double-stranded DNA. At high temperatures, double-stranded regions of the DNA dehybridize and the fluorescence decreases. TFA monitors aptamer melting, leveraging the changes in thermodynamic stability afforded by target binding.

TFA was used to test the binding of HAdV-Seq4 aptamer to HAdV. A solution containing 20 nM of aptamer was annealed at 95 °C and cooled down slowly at room temperature. Then, a mixture of 2 μL of the aptamer solution, 2 μL of SYBR Gold (1:100 dilution), and 15 μL of HAdV solution at different concentrations was added to individual wells. All sets of samples were placed in the qPCR instrument and melting curve data was acquired in triplicate, between 20 °C and 95 °C, at 0.5 °C per min with data collection at 30 s intervals. Fig. S2 shows the melting curves at the different conditions.

A control experiment was carried out in the same conditions but without HAdV-Seq4 aptamer to determine the background signal contribution from just HAdV virus. Also, a negative control was performed by replacing the HAdV-Seq4 aptamer with a nonspecific DNA, containing the same length but a random sequence, to confirm that the detected changes corresponded to the specific

Science Advances Manuscript Template Page 16 of 23

interaction between HAdV-Seq4 aptamer and the infectious HAdV. Finally, a selectivity test was performed by repeating the assay with the HAdV-Seq4 aptamer using a different virus commonly present in water samples, Coxsackievirus.

Microscale Thermophoresis (MST) measurements

Microscale Thermophoresis (MST) was used to test the binding of SARS2-AR10 aptamer with pseudotyped SARS-CoV-2 and other related viruses. A 1:2 serial dilution of 16 samples of the virus with SELEX buffer was prepared covering the concentration range of 3.9×10^8 to 4.8×10^4 copies/mL. To 10 μ L of each of the serial dilutions, 10 μ L of 500 nM stock solution of FAM-functionalized SARS2-AR10 was added and allowed to incubate for 10 min at room temperature. Subsequently, each sample was loaded onto a NanoTemper (Munich, Germany) KM-022 capillary tube and mounted on a NanoTemper Monolith Nt.115 (provided by the UIUC Microbiology Department) capillary tray. Each measurement was tested at a light-emitting diode power of 20% at the "Blue" excitation wavelength setting, with a cold region of 5 s, followed by a hot region of 30 s, until the new hot equilibrium state was observed, followed by 5 more seconds of cold region to observe the regeneration of the fluorescence signal. For each MST measurement, each capillary was subjected to an IR laser power at 40% of its power to record the resulting thermophoretic curves. Each of these measurements included three repeat experiments.

To test the selectivity of the aptamer, the same experiment was performed with UV-inactivated pseudotyped SARS-CoV-2, pseudotyped SARS-CoV-1, pseudotyped H5N1, and 229E coronavirus.

Nanopore fabrication

12 µm polyethylene terephthalate (PET) foils are irradiated at the UNILAC heavy ion accelerator of the GSI Helmholtz Centre for Heavy Ion Research with single GeV Au ion. Each highly energetic ion creates a highly localized damage trail, known as ion-track, along its trajectory through the polymer foil. The ion-track has a diameter of a few nm and can be selectively removed by chemical etching. Chemical etching is performed in a custom, in-house built electrochemical cell, such that the irradiated foil is inserted between two separate compartments. The compartments are filled with 6 M NaOH, and 6 M NaOH + 0.05 % (in volume) Dowfax 2a1, respectively. Etching is performed for 6 minutes at 60 °C, to fabricate bullet-like shaped nanochannels, *i.e.* a combination of longer cylindrical and shorter parabolic segments. Single nanochannels with bullet-like shape exhibit nonlinear current-voltage characteristics due to the asymmetric shape of the reduced size tip and the negative charges stemming from the carboxylate groups generated on the polymer surface during the etching. Average dimensions of the as-obtained bullet-like shaped nanochannels are: (a) tip \leq 55 nm, (b) base: 900 \pm 100 nm, as described previously (39).

Modification of nanopore and immobilization of the aptamer

After etching, the single nanochannel membranes were modified with the HAdV aptamer by EDC/Sulfo-NHS coupling between the carboxylate groups in the nanopore and an amino modified HAdV-Seq4 aptamer. We chose to incorporate the amino modification at the 5' end with the longest linker available from IDT (12 CH₂-groups) to minimize the potential for the nanopore surface to interfere with aptamer binding to its target (NH₂-C₁₂-Aptamer, see Table 1). For HAdV-Seq4 aptamer, we also incorporated the amine modification at the 3' end to compare the effect of the different orientation of the HAdV aptamer on the surface (Fig. S3). In this case, only a shorter linker (6 CH₂-groups) was available from IDT (3AmMO-Aptamer, see Table 1).

Science Advances Manuscript Template Page 17 of 23

The PET single nanochannel membrane was incubated first with 20 mM EDC and 30 mM Sulfo-730 NHS in Reaction Buffer (100 mM MES, pH 5.5) for 45 min at room temperature to form the sulfo-731 732

NHS esters. In the second step, after washing with the same buffer, the membrane is incubated

overnight (≥ 6 hours) with a solution of 2 μ M amino-DNA in Reaction Buffer at room temperature.

NH₂-C₁₂-SARS2-AR10 aptamer was incorporated in the nanopore following the same procedure as for HAdV-Seq4.

735

733

734

736

737 738

739

740 741

742

743 744

745

746 747

748

749

750

751

752

753

754 755

756

757

758

759

760 761

762

763

764 765

766 767

768

769

770

771

772

773

Current-Voltage measurements

Current-voltage (I-V) curves were recorded using a potentiostat (CHI620, CH Instruments) in a four-electrode set up (working, working sense, reference, and counter-electrode). In this way, we can monitor conductance variations arising from changes in the nanochannel and separate them from other processes in solution or on electrode surfaces. Both the working and counter-electrode were platinum wires while the reference and working-sense were commercial silver/silver chloride (Ag/AgCl/3M KCl) electrodes. In all experiments, working and counter electrodes were placed at the tip and base of the channels, respectively. A 0.1 M KCl solution was used as the electrolyte.

Measurement of the virus samples

1.5 mL of the sample containing the virus was incorporated in the compartment facing the base of the aptamer-modified nanochannel, while a SELEX buffer was filled in the compartment facing the nanopore tip. The solutions were incorporated by pipetting into the chambers using a plastic pipette. After incubation for the given time (30 min or 2 hr), the solutions were removed, and the compartments were rinsed with milli-Q water. Then, the 0.1 M KCl electrolyte was inserted in both compartments to record the I-V characteristics between +1 and -1 V at 100 mV/s (3cycles).

In the case of the environmental water and human serum and saliva samples, 15µL of different dilutions of infectious virus (HAdV or pseudotyped SARS-CoV-2) were spiked in 1.5mL of these samples to obtain the final concentration of spiked viruses. The dilutions of infectious virus were prepared using SELEX buffer to dilute the 6x10⁵ pfu/mL HAdV stock solution (in CBS buffer) or 1x10¹¹ copies/mL pseudotyped SARS-CoV-2 stock solution (in PBS buffer). For the environmental water samples, the final viral titers tested were 10, 60, and 600 pfu/mL of HAdV; while for human serum and saliva, 6, 60, and 600 pfu/mL of HAdV were tested. In the case of SARS-CoV-2, the final viral titers tested were $1x10^4$, $1x10^5$, $1x10^6$, and $1x10^7$ copies/mL. For each concentration of virus, 3 replicates are measured using single-use aptamer-nanopore system and independently prepared virus solutions from a virus stock. From these replicates, two of them were done with pooled saliva samples we have purchased and the third replicate was done with individual fresh saliva samples. Not different were observed between these two types of saliva samples.

Rectification efficiency

In all experiments the definition for the rectification efficiency (f_{rec}) is given by,

$$f_{rec} = \pm \left| \frac{I(1V \ or - 1V)}{I(-1V \ or \ 1V)} \right|$$

where the current I in the numerator corresponds to the largest current value in the high conductance state, and the current in the denominator is the lowest current value corresponding to the low conductance state. Additionally, if the higher current corresponds to a negative voltage, the rectification factor is multiplied by -1. This definition simplifies the notation. In order to compare results stemming from different nanopores, a normalized rectification efficiency (freenorm) is

Page 18 of 23 Manuscript Template Science Advances

defined by dividing each f_{rec} from a specific nanochannel by the f_{rec} value in presence of just buffer ($f_{rec,0}$),

$$f_{rec}norm = \frac{f_{rec}}{f_{rec}}$$

In the case of human serum and saliva samples, the f_{rec} norm is calculated by dividing each f_{rec} from a specific nanochannel by the f_{rec} value of that nanochannel in presence of human serum or saliva ($f_{rec,0}$).

Thus, the steady-state I-V curves and the rectification factor obtained based on this curve contain precise information that is essential for quantification and background subtraction to remove potential interference from other species in the sample, that is not possible with other nanopore methods.

References

- 1. D. Jacot, G. Greub, K. Jaton, O. Opota, Viral load of SARS-CoV-2 across patients and compared to other respiratory viruses. *Microbes Infect.* **22**, 617–621 (2020).
- 2. A. Ganguli, A. Mostafa, J. Berger, M. Y. Aydin, F. Sun, S. A. Stewart de Ramirez, E. Valera, B. T. Cunningham, W. P. King, R. Bashir, Rapid isothermal amplification and portable detection system for SARS-CoV-2. *Proc. Natl. Acad. Sci. U. S. A.* 117, 22727–22735 (2020).
- 3. C. Myhrvold, C. A. Freije, J. S. Gootenberg, O. O. Abudayyeh, H. C. Metsky, A. F. Durbin, M. J. Kellner, A. L. Tan, L. M. Paul, L. A. Parham, K. F. Garcia, K. G. Barnes, B. Chak, A. Mondini, M. L. Nogueira, S. Isern, S. F. Michael, I. Lorenzana, N. L. Yozwiak, B. L. MacInnis, I. Bosch, L. Gehrke, F. Zhang, P. C. Sabeti, Field-deployable viral diagnostics using CRISPR-Cas13. *Science*. **360**, 444–448 (2018).
- 4. I. Arevalo-Rodriguez, D. Buitrago-Garcia, D. Simancas-Racines, P. Zambrano-Achig, R. Del Campo, A. Ciapponi, O. Sued, L. Martinez-García, A. W. Rutjes, N. Low, P. M. Bossuyt, J. A. Perez-Molina, J. Zamora, False-negative results of initial RT-PCR assays for COVID-19: A systematic review. *PLoS One.* **15**, e0242958 (2020).
- F. Amanat, D. Stadlbauer, S. Strohmeier, T. H. O. Nguyen, V. Chromikova, M. McMahon, K. Jiang, G. A. Arunkumar, D. Jurczyszak, J. Polanco, M. Bermudez-Gonzalez, G. Kleiner, T. Aydillo, L. Miorin, D. S. Fierer, L. A. Lugo, E. M. Kojic, J. Stoever, S. T. H. Liu, C. Cunningham-Rundles, P. L. Felgner, T. Moran, A. García-Sastre, D. Caplivski, A. C. Cheng, K. Kedzierska, O. Vapalahti, J. M. Hepojoki, V. Simon, F. Krammer, A serological assay to detect SARS-CoV-2 seroconversion in humans. *Nat. Med.* 26, 1033–1036 (2020).
- 6. C. Sheridan, Fast, portable tests come online to curb coronavirus pandemic. *Nat. Biotechnol.* (2020), doi:10.1038/d41587-020-00010-2.
- R. Wölfel, V. M. Corman, W. Guggemos, M. Seilmaier, S. Zange, M. A. Müller, D.
 Niemeyer, T. C. Jones, P. Vollmar, C. Rothe, M. Hoelscher, T. Bleicker, S. Brünink, J.
 Schneider, R. Ehmann, K. Zwirglmaier, C. Drosten, C. Wendtner, Virological assessment of hospitalized patients with COVID-2019. *Nature*. 581, 465–469 (2020).
- 8. R. Service, Coronavirus antigen tests: quick and cheap, but too often wrong? *Science* (2020), doi:10.1126/science.abc9586.
 - 9. R. Weissleder, H. Lee, J. Ko, M. J. Pittet, COVID-19 diagnostics in context. *Sci. Transl. Med.* **12**, 1–7 (2020).
- Handler 10. G. M. Joynt, W. K. Wu, Understanding COVID-19: what does viral RNA load really mean? *Lancet Infect. Dis.* **3099**, 19–20 (2020).
- N. Cook, D. O. Cliver, in *Encyclopedia of Food Microbiology* (Elsevier, 2014; https://linkinghub.elsevier.com/retrieve/pii/B9780123847300003517), vol. 3, pp. 727–731.
- 822 12. S. Khanal, P. Ghimire, A. Dhamoon, The repertoire of adenovirus in human disease: the

Science Advances Manuscript Template Page 19 of 23

innocuous to the deadly. *Biomedicines*. **6**, 30 (2018).

831

832

836

837

841

842

843

844

845

- M. R. Dunn, R. M. Jimenez, J. C. Chaput, Analysis of aptamer discovery and technology. *Nat. Rev. Chem.* **1**, 0076 (2017).
- Z. Shen, Z. Wu, D. Chang, W. Zhang, K. Tram, C. Lee, P. Kim, B. J. Salena, Y. Li, A
 catalytic DNA activated by a specific strain of bacterial pathogen. *Angew. Chemie Int. Ed.* 55, 2431–2434 (2016).
- M. A. Page, J. L. Shisler, B. J. Mariñas, Kinetics of adenovirus type 2 inactivation with free chlorine. *Water Res.* **43**, 2916–2926 (2009).
 - 16. K. Sefah, D. Shangguan, X. Xiong, M. B. O'Donoghue, W. Tan, Development of DNA aptamers using Cell-SELEX. *Nat. Protoc.* **5**, 1169–85 (2010).
- N. Kacherovsky, I. I. Cardle, E. L. Cheng, J. L. Yu, M. L. Baldwin, S. J. Salipante, M. C. Jensen, S. H. Pun, Traceless aptamer-mediated isolation of CD8+ T cells for chimeric antigen receptor T-cell therapy. *Nat. Biomed. Eng.* **3**, 783–795 (2019).
 - 18. Q. Pan, F. Luo, M. Liu, X. L. Zhang, Oligonucleotide aptamers: promising and powerful diagnostic and therapeutic tools for infectious diseases. *J. Infect.* 77, 83–98 (2018).
- 19. C. L. A. Hamula, H. Peng, Z. Wang, G. J. Tyrrell, X.-F. Li, X. C. Le, An improved SELEX technique for selection of DNA aptamers binding to M-type 11 of Streptococcus pyogenes.

 Methods. 97, 51–57 (2016).
 - 20. A. M. Gall, J. L. Shisler, B. J. Mariñas, Analysis of the viral replication cycle of adenovirus serotype 2 after inactivation by free chlorine. *Environ. Sci. Technol.* **49**, 4584–90 (2015).
 - 21. B. Vazquez-Bravo, K. Gonçalves, J. L. Shisler, B. J. Mariñas, Adenovirus Replication Cycle Disruption from Exposure to Polychromatic Ultraviolet Irradiation. *Environ. Sci. Technol.* **52**, 3652–3659 (2018).
- V. A. Avanzato, M. J. Matson, S. N. Seifert, R. Pryce, B. N. Williamson, S. L. Anzick, K. Barbian, S. D. Judson, E. R. Fischer, C. Martens, T. A. Bowden, E. de Wit, F. X. Riedo, V. J. Munster, Case study: prolonged infectious SARS-CoV-2 shedding from an asymptomatic immunocompromised individual with cancer. *Cell.* **183**, 1901-1912.e9 (2020).
- Z. Luo, L. He, J. Wang, X. Fang, L. Zhang, Developing a combined strategy for monitoring the progress of aptamer selection. *Analyst.* **142**, 3136–3139 (2017).
- K. K. Alam, J. L. Chang, D. H. Burke, FASTAptamer: A bioinformatic toolkit for highthroughput sequence analysis of combinatorial selections. *Mol. Ther. - Nucleic Acids.* **4**, e230 (2015).
- M. R. Gotrik, T. A. Feagin, A. T. Csordas, M. A. Nakamoto, H. T. Soh, Advancements in aptamer discovery technologies. *Acc. Chem. Res.* **49**, 1903–1910 (2016).
- C. Bai, Z. Lu, H. Jiang, Z. Yang, X. Liu, H. Ding, H. Li, J. Dong, A. Huang, T. Fang, Y. Jiang, L. Zhu, X. Lou, S. Li, N. Shao, Aptamer selection and application in multivalent binding-based electrical impedance detection of inactivated H1N1 virus. *Biosens*.
 Bioelectron. 110, 162–167 (2018).
- T. Lu, Q. Ma, W. Yan, Y. Wang, Y. Zhang, L. Zhao, H. Chen, Selection of an aptamer against Muscovy duck parvovirus for highly sensitive rapid visual detection by label-free aptasensor. *Talanta*. **176**, 214–220 (2018).
- B. I. Escudero-Abarca, S. H. Suh, M. D. Moore, H. P. Dwivedi, L. A. Jaykus, Selection, characterization and application of nucleic acid aptamers for the capture and detection of human norovirus strains. *PLoS One.* **9**, e106805 (2014).
- T. R. Damase, T. A. Miura, C. E. Parent, P. B. Allen, Application of the open qPCR instrument for the in vitro selection of DNA aptamers against epidermal growth factor receptor and Drosophila C virus. *ACS Comb. Sci.* **20**, 45–54 (2018).
- 30. J. Hu, J. Kim, C. J. Easley, Quantifying aptamer–protein binding via thermofluorimetric analysis. *Anal. Methods.* **7**, 7358–7362 (2015).

Science Advances Manuscript Template Page 20 of 23

- 31. G. Pérez-Mitta, A. G. Albesa, C. Trautmann, M. E. Toimil-Molares, O. Azzaroni,
 Bioinspired integrated nanosystems based on solid-state nanopores: "iontronic"
 transduction of biological, chemical and physical stimuli. *Chem. Sci.* **8**, 890–913 (2017).
- 32. U. F. Keyser, Enhancing nanopore sensing with DNA nanotechnology. *Nat. Nanotechnol.* 11, 106–108 (2016).
- 33. A. Arima, I. H. Harlisa, T. Yoshida, M. Tsutsui, M. Tanaka, K. Yokota, W. Tonomura, J. Yasuda, M. Taniguchi, T. Washio, M. Okochi, T. Kawai, Identifying single viruses using biorecognition solid-state nanopores. *J. Am. Chem. Soc.* **140**, 16834–16841 (2018).

884

885 886

887

888

889

890

891892

893

894

895

899

900

901

902

903

904

905

922

- 34. Z. Zhu, D. Wang, Y. Tian, L. Jiang, Ion/molecule transportation in nanopores and nanochannels: from critical principles to diverse functions. *J. Am. Chem. Soc.* **141**, 8658–8669 (2019).
 - 35. Z. Sun, T. Liao, Y. Zhang, J. Shu, H. Zhang, G.-J. Zhang, Biomimetic nanochannels based biosensor for ultrasensitive and label-free detection of nucleic acids. *Biosens. Bioelectron.* **86**, 194–201 (2016).
 - 36. T. Liao, X. Li, Q. Tong, K. Zou, H. Zhang, L. Tang, Z. Sun, G. J. Zhang, Ultrasensitive detection of microRNAs with morpholino-functionalized nanochannel biosensor. *Anal. Chem.* **89**, 5511–5518 (2017).
 - 37. L. Mayne, C.-Y. Lin, S. D. R. Christie, Z. S. Siwy, M. Platt, The design and characterization of multifunctional aptamer nanopore sensors. *ACS Nano*. **12**, 4844–4852 (2018).
 - 38. P. Y. Apel, I. V. Blonskaya, S. N. Dmitriev, O. L. Orelovitch, A. Presz, B. A. Sartowska, Fabrication of nanopores in polymer foils with surfactant-controlled longitudinal profiles. *Nanotechnology.* **18**, 305302 (2007).
- 39. G. Pérez-Mitta, A. S. Peinetti, M. L. Cortez, M. E. Toimil-Molares, C. Trautmann, O. Azzaroni, Highly sensitive biosensing with solid-state nanopores displaying enzymatically reconfigurable rectification properties. *Nano Lett.* **18**, 3303–3310 (2018).
 - 40. X. Hou, W. Guo, F. Xia, F.-Q. Nie, H. Dong, Y. Tian, L. Wen, L. Wang, L. Cao, Y. Yang, J. Xue, Y. Song, Y. Wang, D. Liu, L. Jiang, A biomimetic potassium responsive nanochannel: G-quadruplex DNA conformational switching in a synthetic nanopore. *J. Am. Chem. Soc.* **131**, 7800–7805 (2009).
 - 41. Y. Guo, J. Tisoncik, S. McReynolds, M. Farzan, B. S. Prabhakar, T. Gallagher, L. Rong, M. Caffrey, Identification of a new region of SARS-CoV S protein critical for viral entry. *J. Mol. Biol.* **394**, 600–605 (2009).
- 906 42. Q. Cui, H. Cheng, R. Xiong, G. Zhang, R. Du, M. Anantpadma, R. Davey, L. Rong, Identification of diaryl-quinoline compounds as entry inhibitors of Ebola virus. *Viruses*. **10**, 678 (2018).
- 43. X. Ou, Y. Liu, X. Lei, P. Li, D. Mi, L. Ren, L. Guo, R. Guo, T. Chen, J. Hu, Z. Xiang, Z.
 Mu, X. Chen, J. Chen, K. Hu, Q. Jin, J. Wang, Z. Qian, Characterization of spike
 glycoprotein of SARS-CoV-2 on virus entry and its immune cross-reactivity with SARS-CoV. *Nat. Commun.* 11, 1620 (2020).
- J. P. Broughton, W. Deng, C. L. Fasching, J. Singh, Y. Charles, J. S. Chen, M. Biosciences,
 S. S. Francisco, S. Francisco, A protocol for rapid detection of SARS-CoV-2
 using CRISPR: SARS-CoV-2 DETECTR Mammoth Biosciences, 1–9 (2020).
- V. L. Dao Thi, K. Herbst, K. Boerner, M. Meurer, L. P. Kremer, D. Kirrmaier, A.
 Freistaedter, D. Papagiannidis, C. Galmozzi, M. L. Stanifer, S. Boulant, S. Klein, P.
 Chlanda, D. Khalid, I. B. Miranda, P. Schnitzler, H.-G. Kräusslich, M. Knop, S. Anders, A
 colorimetric RT-LAMP assay and LAMP-sequencing for detecting SARS-CoV-2 RNA in
- clinical samples. *Sci. Transl. Med.* 7075, 1–20 (2020).
 P. S. Kwon, S. Ren, S. Kwon, M. E. Kizer, L. Kuo, M. Xie, D. Zhu, F. Zhou, F. Zhang, D.

Science Advances Manuscript Template Page 21 of 23

Kim, K. Fraser, L. D. Kramer, N. C. Seeman, J. S. Dordick, R. J. Linhardt, J. Chao, X.

- Wang, Designer DNA architecture offers precise and multivalent spatial patternrecognition for viral sensing and inhibition. *Nat. Chem.* **12**, 26–35 (2020).
- 925 47. M. Tagliazucchi, O. Azzaroni, I. Szleifer, Responsive polymers end-tethered in solid-state nanochannels: When nanoconfinement really matters. *J. Am. Chem. Soc.* **132**, 12404–927 12411 (2010).
 - 48. F. M. Gilles, M. Tagliazucchi, O. Azzaroni, I. Szleifer, Ionic conductance of polyelectrolyte-modified nanochannels: nanoconfinement effects on the coupled protonation equilibria of polyprotic brushes. *J. Phys. Chem. C.* **120**, 4789–4798 (2016).
 - 49. Y. Song, J. Song, X. Wei, M. Huang, M. Sun, L. Zhu, B. Lin, H. Shen, Z. Zhu, C. Yang, Discovery of aptamers targeting the receptor-binding domain of the SARS-CoV-2 spike glycoprotein. *Anal. Chem.* **92**, 9895–9900 (2020).
 - 50. A. Schmitz, A. Weber, M. Bayin, S. Breuers, V. Fieberg, M. Famulok, G. Mayer, A SARS-CoV-2 spike binding DNA aptamer that inhibits pseudovirus infection by an RBD-independent mechanism. *Angew. Chemie Int. Ed.* **60**, 10279–10285 (2021).
 - 51. M. Sun, S. Liu, X. Wei, S. Wan, M. Huang, T. Song, Y. Lu, X. Weng, Z. Lin, H. Chen, Y. Song, C. Yang, Aptamer blocking strategy inhibits SARS-CoV-2 virus infection. *Angew. Chemie Int. Ed.* **60**, 10266–10272 (2021).
 - 52. E. W. Rice, R. B. Baird, A. D. Eaton, Eds., *Standard Methods for the Examination of Water and Wastewater* (American Public Health Association, ed. 23rd, 2017).
 - 53. J. R. Bolton, K. G. Linden, Standardization of methods for fluence (UV Dose) determination in bench-scale UV experiments. *J. Environ. Eng.* **129**, 209–215 (2003).
 - 54. T. L. Cromeans, X. Lu, D. D. Erdman, C. D. Humphrey, V. R. Hill, Development of plaque assays for adenoviruses 40 and 41. *J. Virol. Methods.* **151**, 140–145 (2008).
 - 55. A. M. Gall, J. L. Shisler, B. J. Mariñas, Inactivation kinetics and replication cycle inhibition of adenovirus by monochloramine. *Environ. Sci. Technol. Lett.* **49**, 4584–4590 (2016).
 - 56. L. Zhang, X. Fang, X. Liu, H. Ou, H. Zhang, J. Wang, Q. Li, H. Cheng, W. Zhang, Z. Luo, Discovery of sandwich type COVID-19 nucleocapsid protein DNA aptamers. *Chem. Commun.* **56**, 10235–10238 (2020).

Acknowledgments

We thank Kelly Goncalves for preparing the initial adenovirus samples, the Urbana & Champaign Sanitary District (IL, US) for providing the wastewater samples, and the Panyodoli Secondary School in Kiryandongo District (Uganda) for providing the borehole water samples. Thomas Gallagher at Loyola University supplied the 229E-CoV, Huh-7 cell line, the SARS-CoV-2 Sprotein plasmid, and the SARS-CoV-1 S-protein plasmid. HTS was performed by the DNA Services Lab of the Roy J. Carver Biotechnology Center at UIUC and we thank Dr. Alvaro Hernandez and Dr. Chris Wright with their help in advising for the DNA library preparation and for performing the Illumina sequencing.

Funding. This work was supported by a RAPID grant from the National Science Foundation (CBET 20-29215) and a seed grant from the Institute for Sustainability, Energy, and Environment at University of Illinois at Urbana-Champaign and Illinois-JITRI Institute (JITRI 23965). A.S.P. thanks the PEW Latin American Fellowship for financial support. The irradiated PET foils are part of the experiment UMAT, which was performed at the beam line X0 at the GSI Helmhotzzentrum fuer Schwerionenforschung, Darmstadt (Germany) in the frame of FAIR Phase-0. O.A. acknowledges financial support from CONICET (PIP0370) and ANPCyT (PICT-2016-1680 and PICT-2017-1523).

Science Advances Manuscript Template Page 22 of 23

Author contributions. A.S.P., B.M. and Y.L. conceptualized the study. A.S.P., O.A., B.M., L.R. and Y.L designed methodology. A.S.P. and R.J.L. performed and analyzed the experiments related with aptamer SELEX and nanopore measurements. A.S.P., Y.W., Y.M. and G.T.P. performed binding affinity assay experiments. W.C. and L.C. prepared the virus and pseudovirus samples and performed microbiology experiments. O.A., M.E.T-M and C.T. synthesized the solid-state nanopore and designed the nanopore measurement set-up. Y.L. was responsible for project supervision, direction and resource acquisition. A.S.P., R.J.L., and Y.L. wrote the manuscript and all authors edited and reviewed it.

Competing interests. A patent based on this work (US 63/027,799) has been filed. Y. L. is a cofounder and board member of ANDalyze, Inc. and GlucoSentient, Inc.

Data and materials availability: All data needed to evaluate the conclusions in the paper are present in the main text or the Supplementary Materials.

Supplementary Materials

 Supplementary Text 1 to 3 Figs. S1 to S19 Table S1

Science Advances Manuscript Template Page 23 of 23



advances.sciencemag.org/cgi/content/full/sciadv.[ms.no.]/DC1

Supplementary Materials for

Direct detection of human adenovirus and SARS-CoV-2 with ability to inform infectivity using a DNA aptamer-nanopore sensor

Ana Sol Peinetti^{1,†}, Ryan J. Lake¹, Wen Cong², Laura Cooper³, Yuting Wu¹, Yuan Ma¹, Gregory T. Pawel¹, María Eugenia Toimil-Molares^{4,*}, Christina Trautmann^{4,5}, Lijun Rong^{3,*} Benito Mariñas^{2,*} Omar Azzaroni^{6,*} and Yi Lu^{1,*}

*Corresponding author. Email: yi-lu@illinois.edu; azzaroni@inifta.unlp.edu.ar; marinas@illinois.edu; lijun@uic.edu, m.e.toimilmolares@gsi.de

This PDF file includes:

Supplementary Text 1 to 3 Figs. S1 to S19 Tables S1

Supplementary Text

Supplementary Text 1. A comparison between plaque assays, qPCR, and our aptamernanopore sensor.

We have quantified the infectious HAdV concentration using plaque assays and benchmarked our results with this, as it is still considered the gold standard method to quantify infectious virus, since simpler and more recently developed methods like qPCR and immunoassays are not capable of distinguishing noninfectious/inactivated virus from active virus (11). It is likely that the efficiency of infectivity determined by plaque assay is lower than 100% because some infective viruses that reach the surface of host cells in the plaque assay might not locate protein receptors involved in the initial attachment steps of the infection cycle, ultimately resulting in the formation of plaques. Although to date there is no method to determine what portion of the overall concentration of infective virions is obtained by plaque assay, a comparison could be made between results from plaque assays and qPCR measurements of genome copies in the same samples. In a previous study, members of our team quantified (in triplicate) HAdV-2 samples with both plaque assay and qPCR (55). The results reproduced in Table S1 reveal a ratio of ≈150 copies/pfu. Unfortunately, the number of genome copies could not be considered to directly correspond to infective viruses because some copies could be associated with incompletely assembled virions not capable of infection. An important point revealed by the stirring test data in Fig. S7 is that the regression has a stronger linear dependence compared to that of the tests without stirring. Extrapolation of the linear regression to freenorm=1 would result in an intercept of approximately 0.1 pfu/mL, suggesting that the sensor would have a sensitivity approximately one order of magnitude higher than that of the plaque assay. These results suggest that 1/15 genome copies could potentially correspond to infective viruses. Such a possibility is plausible because our aptamer method is targeting capsid proteins that are synthesized in the final steps of the infection cycle, and so the possibility that the signal corresponds to infective viruses is higher. If so, the concentration of infectious virions would be ten times that determined by plaque assay. In terms of our assay, this result indicates that, in the nanopore, we are not necessarily detecting a single infective particle in the sample, but the signal corresponds to an order of magnitude higher number, indicating that we reach the same or higher detection limit as the gold standard method, plaque assay, with a rapid and simple test. Moreover, this result highlights that plaque assays likely underestimate infectious virus concentration.

Table S1. Comparison between qPCR and plaque assay quantification of HAdV-2 samples. The number of DNA copies is measured by a 105-bp amplicon in the E1A gene.

Experiment	pfu/mL	DNA copies/mL	DNA copies/pfu
MC1	1.02 x10 ⁶	1.35 x10 ⁸	131
MC2	9.87 x10 ⁵	1.45 x10 ⁸	147
MC3	7.62×10^5	1.40 x10 ⁸	184
		Average:	154

Supplementary Text 2. Determination of detection and quantification limits.

Based on the linear regression obtained (Fig. S6a), it is possible to define the limit of detection as LoD= $3*\sigma/m$, and the quantification limit as LoQ= $10*\sigma/m$, where m is the slope of the linear calibration (m = 0.123) and σ is the standard deviation of the intercept (σ = 0.0076). Then, to obtain the LoD and LoQ in pfu/mL units, we calculate the antilogarithm, because the linear regression is obtained from a logarithm scale in the x axis. Thus, the LoD = 1.5 pfu/mL and LoQ = 4 pfu/mL. We have also compared, using a two-tailed Student's t test, the mean of the freenorm signal obtained for 1 pfu/mL of infectious HAdV with a) the mean freenorm value for different concentrations of infectious HAdV when no aptamer is grafted in the nanopore, and b) the mean freenorm for different concentrations of noninfectious HAdV after immobilization of the aptamer in the nanopore. We observed in both cases that these values are significantly different to the freenorm for 1 pfu/mL of infectious HAdV, with at least 99.9% and 99% confidence, respectively (Fig. S6). Thus, 1 pfu/mL of HAdV is indeed producing a signal distinguishable from these blanks.

Supplementary Text 3. Choice of Lentivirus Pseudotyped with SARS-CoV-2 S protein as the SELEX target.

It had previously been demonstrated that the S protein of SARS-CoV-1 was a good target for recognition, especially since it is the primary surface protein responsible for entry into cells, so the S protein of SARS-CoV-2 was deemed the most suitable target due to its similarity to SARS-CoV-1 (it interacts with the same ACE2 receptor for entry into cells). Other groups have already performed SELEX against the isolated S protein or RBD domain of the S protein of SARS-CoV-2 (49-51), as well as against the N protein (56). Because of our prior success in using whole virus SELEX to isolate the HAdV, we wanted to use a whole viral mimic of SARS-CoV-2 to better replicate the native state of the S protein. For instance, it is known that the S protein forms trimer structures when incorporated into the viral envelope, so using a solubilized S protein in its monomer form loses a significant amount of quaternary structure that could be used by aptamers for better recognition or may even inhibit binding of aptamers that have been selected against the solubilized protein. Other researchers have recently developed variations of the SARS-CoV-2 S protein that allow it to trimerize in its soluble form, but this target is still significantly different from the membrane bound S proteins found in the native system. Furthermore, the S protein in the pseudotyped virus is expressed as a glycoprotein with the same sugar modifications as in the SARS-CoV-2. Because of all these considerations, we desired to use a pseudotyped virus, in which a different virus is used as a backbone, which is incorporated with the SARS-CoV-2 S protein to mimic its native state within the viral envelope.

The Rong lab has extensive experience in creating lentivirus-based pseudoviruses, including for the SARS-CoV-1 S protein. Based on this expertise, we were able to create lentivirus pseudotyped with the SARS-CoV-2 S protein in a rapid manner, allowing us to use it as the target for our SELEX and for testing our nanopore sensor at BSL-2 levels while still maintaining high similarity to the S protein in its native viral envelope.

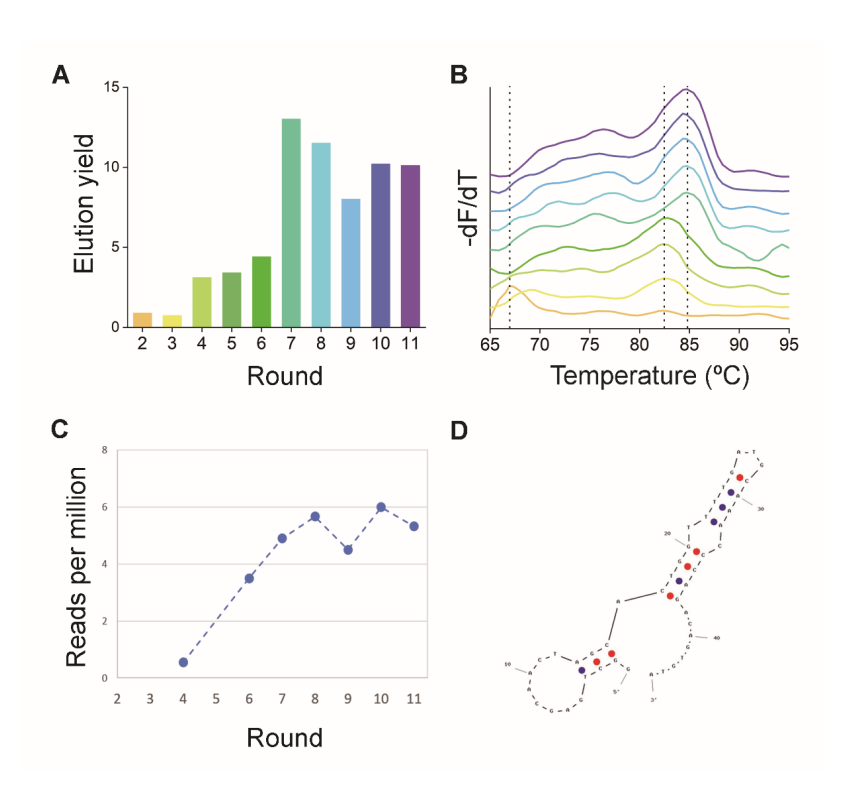


Fig. S1. *In-vitro* **selection of infectious HAdV-specific aptamers. (A)** Monitoring the progress of the SELEX process by quantification of the elution yield, i.e., bound ssDNA over total added ssDNA, using qPCR. **(B)** Melting curve for the different pools during HAdV aptamer selection. After round 3 (yellow), a peak at higher melting temperature (Tm) appeared and shifted from 82 °C in the middle rounds to 85 °C at round 7 (green), with its intensity increasing with subsequent rounds, suggesting that the DNA pool has converged from mostly random sequences with low Tm to more conserved sequences with higher Tm. **(C)** Reads per million (RPM) obtained from analysis of the HTS data for the HAdV-Seq4 sequence as a function of the selection rounds, using FASTAptamer-Count. **(D)** The predicted most stable secondary structure of the aptamer based on the UNAFold software. Calculations were made at 25 °C, 100 mM NaCl and 2 mM MgCl₂.

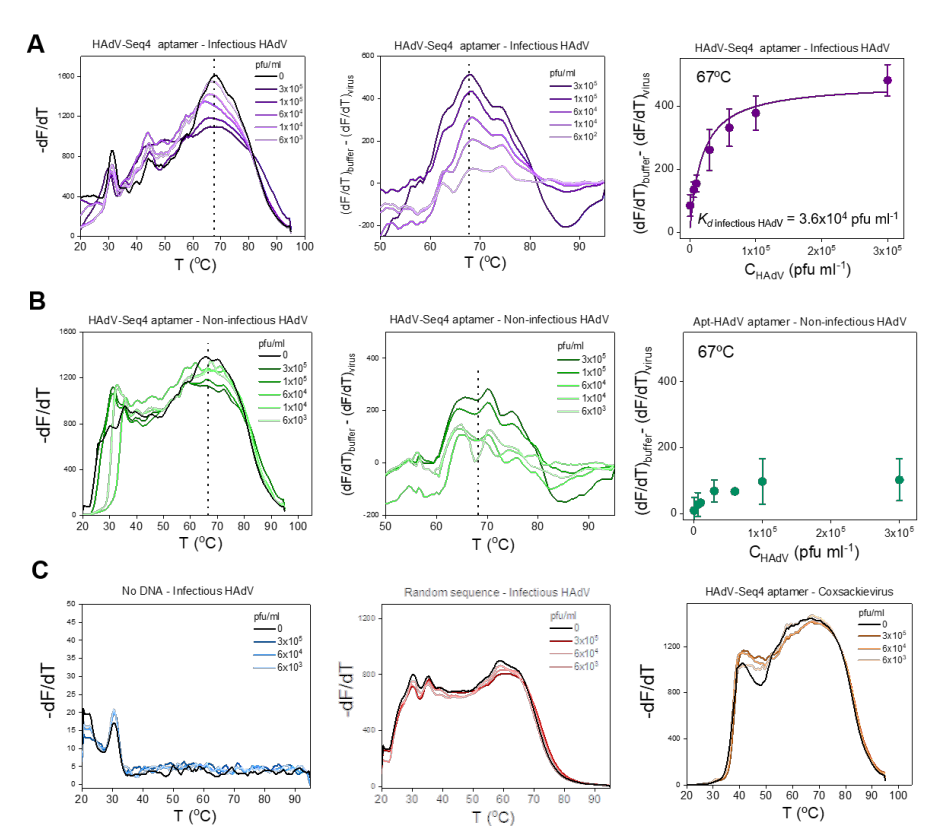


Fig. S2. Thermofluorimetric analysis (TFA) of binding interaction of HAdV-Seq4 aptamer with HAdV using qPCR. (A) From left to right, for infectious HAdV: TFA melt curves; difference of the melt curve between 0 pfu/mL virus and different concentrations of HAdV; and binding curve at 67 °C in presence of 20 nM of HAdV-Seq4 aptamer based on triplicate data. We observed that the peak around 67 °C changes with different concentrations of infectious HAdV, compared with the aptamer solution that does not contain the virus (just buffer, black line). Then, the change in the signal at 67 °C was used to obtain the binding curve, by subtracting the signal without the virus, (dF/dT)_{buffer}, and the signal with different concentration of virus, (dF/dT)_{virus}. (B) Same as (A) but for non-infectious HAdV. In this case, no significant change is observed at 67 °C or other temperature. (C) TFA melt curve for different negative controls: infectious HAdV without DNA, infectious HAdV with 20 nM of a random sequence with the same length of the HAdV-Seq4 aptamer, and coxsackievirus with 20 nM of HAdV-Seq4 aptamer.

√ Deleted: and

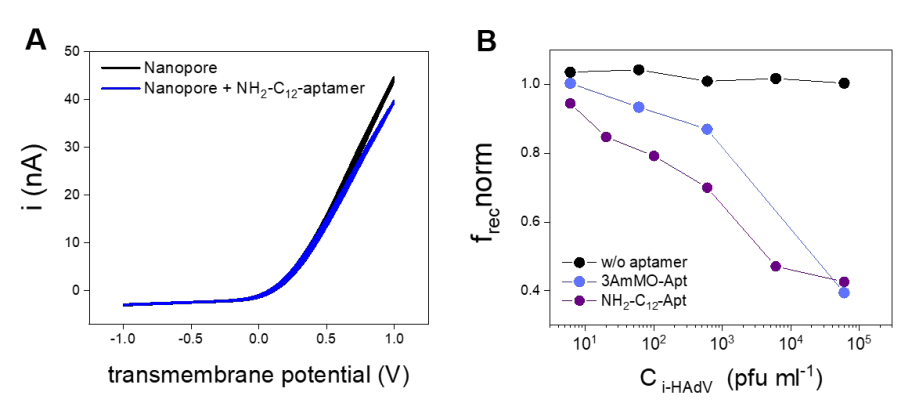


Fig. S3. Modification of nanopore inner surface with HAdV aptamer. (A) I-V curves of a nanopore system before (black) and after (blue) modification with NH₂-C₁₂-aptamer. (B) Normalized rectification efficiencies versus logarithm of the infectious HAdV concentration obtained for different amino modifications of the HAdV aptamer. To prevent the nanopore surface from interfering with the aptamer binding to its target, we added a spacer between the amine group and the aptamer. Also, the effect of different orientations of the HAdV aptamer on the surface was studied by introducing the amino modification on different ends of the sequence. Black corresponds to the nanopore without incorporation of the aptamer. Light blue corresponds to the nanopore modified with 3AmMO-aptamer (3' modification), and purple with NH₂-C₁₂-aptamer (5' modification). We found that the modification at 5' end with the longer spacer improved the sensitivity.

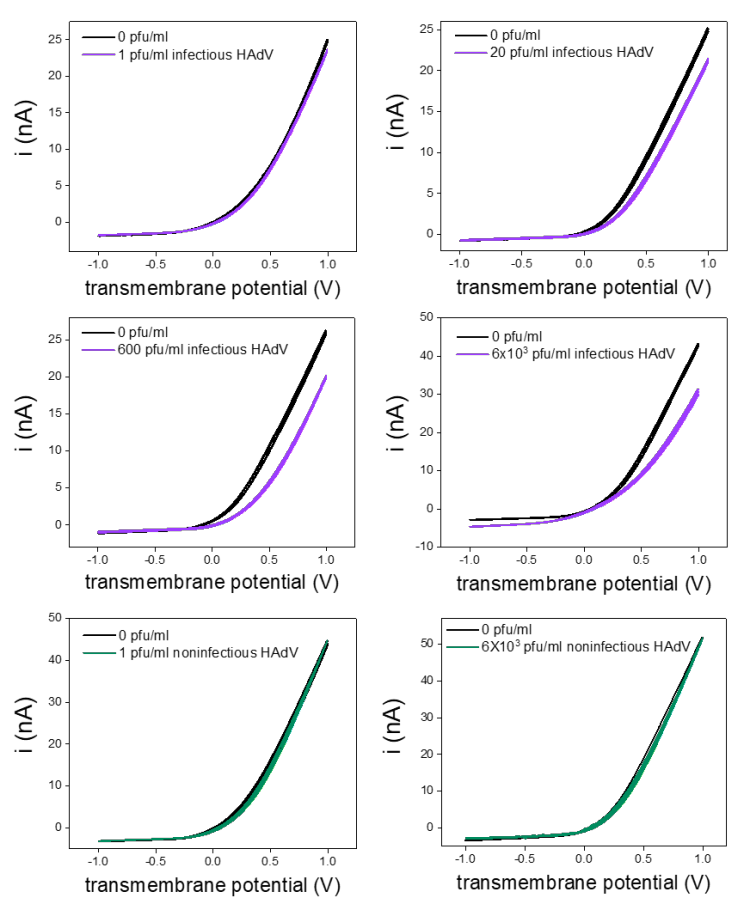


Fig. S4. I-V curves for different nanopores modified with NH₂-C₁₂-aptamer. Black corresponds to incubation of the aptamer-nanopore system with buffer (without virus, 0 pfu/mL) and, purple and green lines correspond to incubations with different concentrations of infectious HAdV or noninfectious HAdV, respectively. Comparing the differences in the I-V curves without virus and with virus for the same membrane, even for a high concentration $(6\times10^3~\text{pfu/mL})$ of noninfectious HAdV, no changes were observed, while for 1 pfu/mL of infectious virus there is a decrease in the current at 1 V.

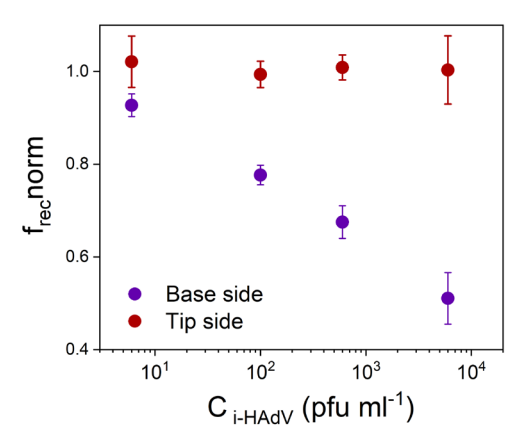


Fig. S5. Effect of virus incubation on different sides of the asymmetrical nanopore on the aptamer-nanopore system performance. Normalized rectification factor versus logarithm of the infectious HAdV concentration after 30 min incubation of the virus solution facing the base side of the nanopore (purple) and facing the tip side (red). No changes in the f_{rec} norm are observed when the virus sample is applied to the reservoir facing the narrow side (tip) of the nanopore. This indicates that the virus needs to be able to enter the nanopore to bind to the aptamer coating the inner surface of the nanopores. Due to the reduced tip size, this is possible only from the base. Tip diameter < 50 nm, base diameter: \approx 900 nm.

Commented [LY1]: Do you mean "immobilization" or "binding"?

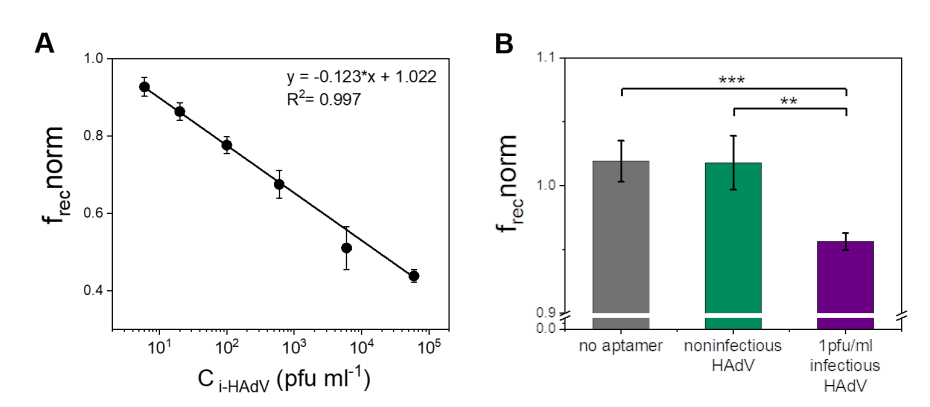


Fig. S6. Limit of detection and sensitivity of the aptamer-nanopore system to detect HAdV. (A) Linear dependence of normalized rectification efficiencies versus logarithm of infectious HAdV concentration with linear fitting. Each data point represents the mean and standard deviation of 3 replicates. (B) The aptamer-nanopore system can detect 1 pfu/mL of infectious HAdV. Normalized rectification efficiency of 1pfu/mL of infectious HAdV after aptamer immobilization on the nanopore (purple). Grey represents the mean and SD of f_{rec} norm for the different concentrations of infectious HAdV showed in Fig. 2b when no aptamer is grafted in the nanopore, while green represents the mean and SD of f_{rec} norm for the different concentrations of noninfectious HAdV showed in Fig. 2b after immobilization of the aptamer in the nanopore. two-tailed Student's t test; **p<0.01, ***p<0.001, bars represent mean \pm SD.

Commented [LY2]: Do you mean "selectivity"? LOD is similar to sensitivity.

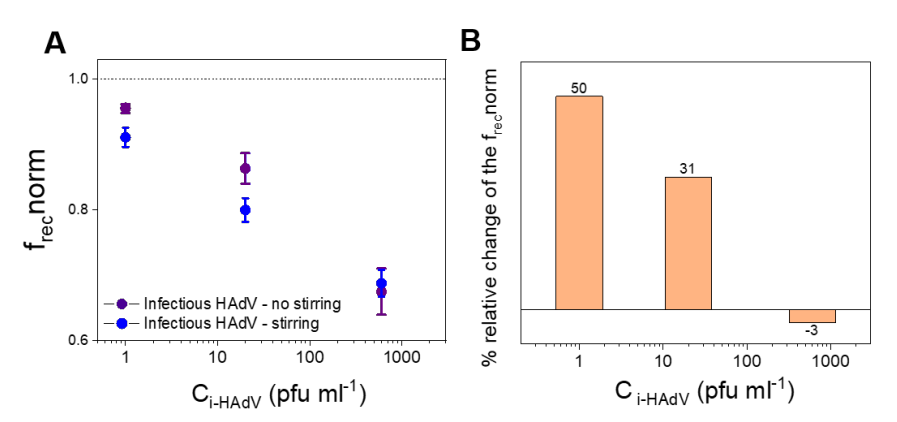


Fig. S7. Effect of stirring during virus incubation on the aptamer-nanopore system performance. (A) Normalized rectification factor versus logarithm of the infectious HAdV concentration after 30 min incubation of the virus solution with the aptamer-nanopore without stirring (purple) or with magnetic stirring (blue). (B) Relative change of the freenorm (defined as the percent change of 1-freenorm) when stirring is added compared with the relative freenorm without stirring, for different concentrations of infectious HAdV. The larger changes are observed for lower infectious HAdV concentrations, and at 600pfu/mL, no significant changes are observed.

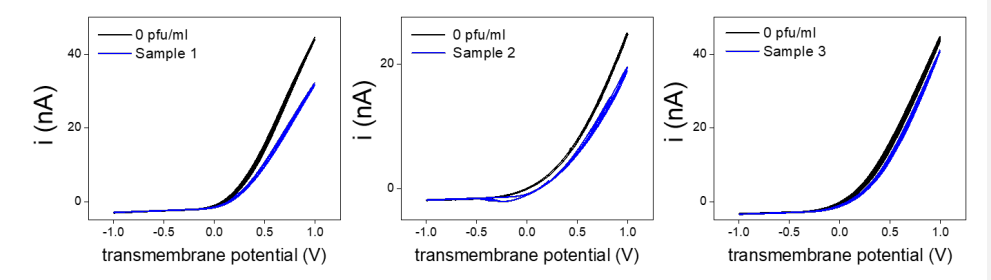


Fig. S8. Detection of infectious HAdV in a buffer solution containing a mixture of infectious and non-infectious HAdV. I-V curves for 3 samples prepared by treating an infectious HAdV sample $(7.2 \times 10^3 \text{ pfu/mL})$ with free chlorine and taking aliquots at different timepoints to obtain different degrees of inactivation with the same total amount of virus: 90% (sample 1), 99% (sample 2), and 99.9% (sample 3). The differences in the f_{rec} indicate that the aptamer-nanopore sensor can detect different infectious HAdV concentrations even when the total amount of virus is the same within different samples.

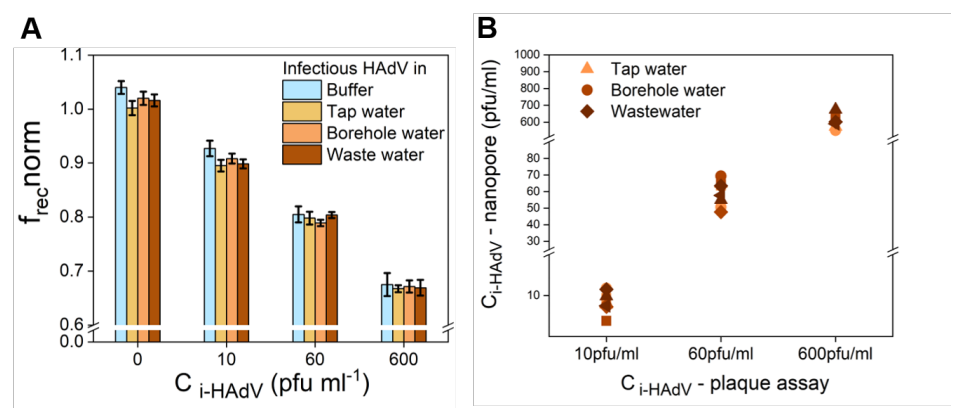


Fig. S9. Detection of infectious HAdV in different real water samples. (A) Normalized rectification efficiency obtained for different concentrations of infectious HAdV that were spiked in drinking water and wastewater. The f_{rec} norm measured for the same concentration of infectious virus in buffer (blue) was included for comparison. n=3, technical replicates (mean \pm SD). (B) Individual values for each concentration (triplicate) for different environmental water samples.

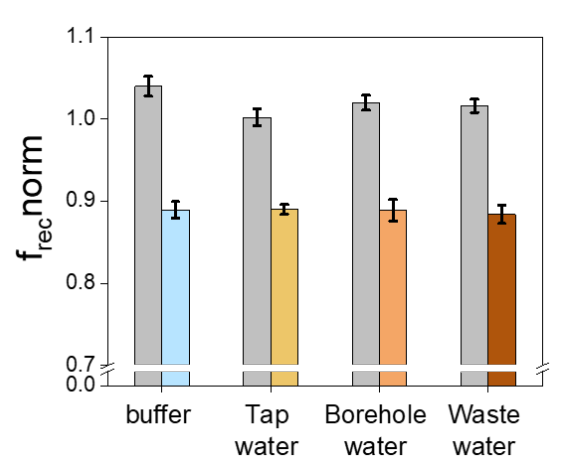


Fig. S10. Detection of infectious HAdV in different real water samples containing a mixture of infectious and non-infectious HAdV. Normalized rectification efficiency obtained for different water samples in presence of non HAdV (gray) and in a solution of HAdV with 99.9% inactivation (mixture of infectious and non-infectious viruses). n=3, technical replicates (mean \pm SD).

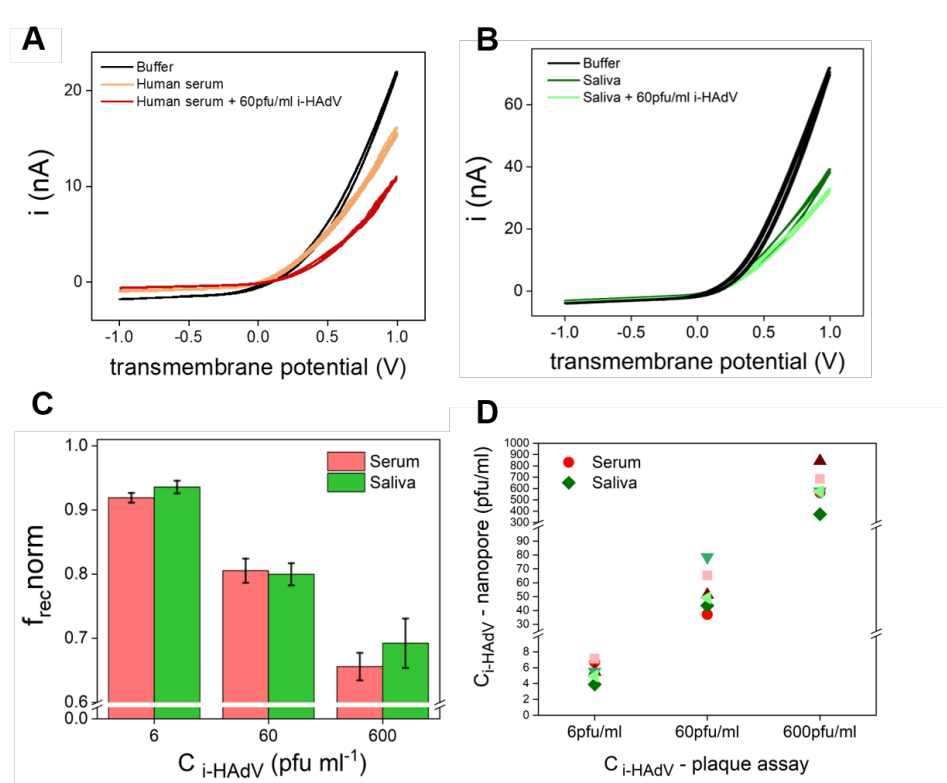


Fig. S11. Detection of infectious HAdV in different biological samples. (A) I-V curves for a human serum sample before (yellow) and after (red) being spiked with 60 pfu/mL infectious HAdV. There is a change in the I-V curve when the nanopore is incubated in human serum compared with the curve after incubation with buffer (black). To take these differences into account, the f_{rec} for the human serum samples with different concentrations of infectious HAdV were normalized by the measurement after incubation in human serum, instead of buffer. **(B)** I-V curves for a human saliva sample before (dark green) and after (light green) being spiked with 60 pfu/mL infectious HAdV. **(C)** Normalized rectification efficiency obtained for human serum and saliva samples spiked with different concentrations of infectious HAdV. n=3, technical replicates (mean ± SD). **(D)** Individual values for each concentration (triplicate) for different biological samples.

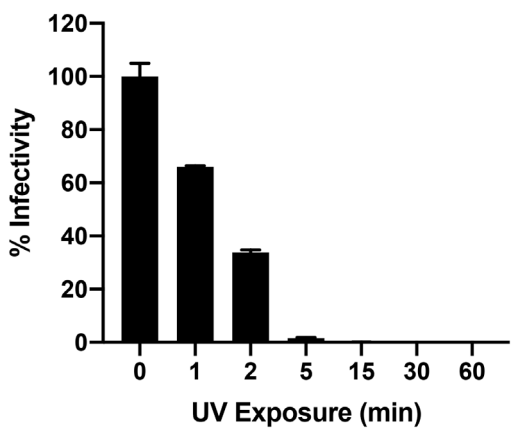


Fig. S12. Monitoring the UV-light inactivation of SARS-CoV-2 pseudovirus at different exposure times by a luciferase assay. In the case of pseudotyped particles, it is not possible to perform a plaque assay.

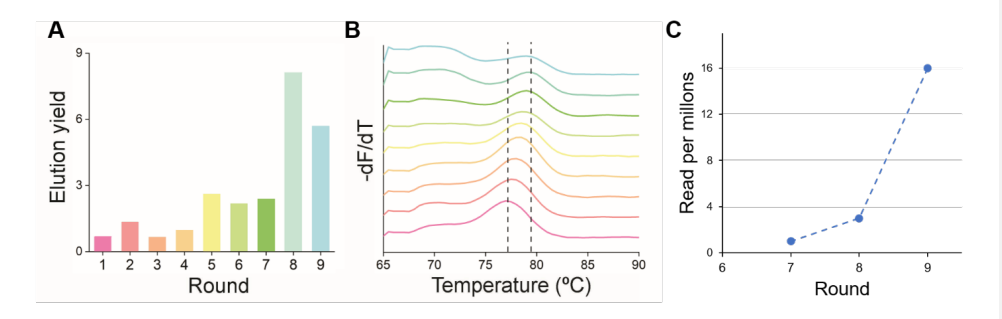


Fig. S13. *In-vitro* **selection of infectious SARS-CoV-2-specific aptamers.** (A) Monitoring the progress of SELEX process by quantification of the elution yield, i.e., the bound ssDNA over the added ssDNA, using qPCR. (B) Melting curve for the different pools during SARS-CoV-2 aptamer selection. The peak at high Tm shifted from 77°C to 79°C, suggesting that the DNA pool has converged from random sequences with low Tm to more conserved sequences with higher Tm. The colors correspond to the colors of the rounds in a. (C) Reads per millions (RPM) obtained by analysis of the HTS data for SARS2-AR10 sequence as a function of the selection rounds, using FASTAptamer-Count.

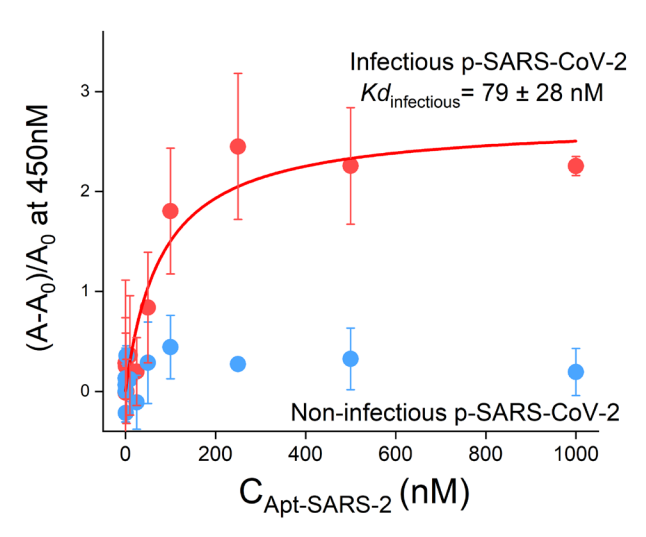


Fig. S14. Binding curves of SARS2-AR10 aptamer and pseudotyped SARS-CoV-2 using ELONA assay. 5×10^8 copies/mL of pseudotyped SARS-CoV-2 are immobilized on a 96-well plate. The dissociation constant (K_d) of SARS2-AR10 sequence for the active pseudotyped SARS-CoV-2 is 79 nM, while no change in the absorbance at 450nm is observed for the inactive pseudotyped SARS-CoV-2. n = 3 technical replicates (mean \pm SD).

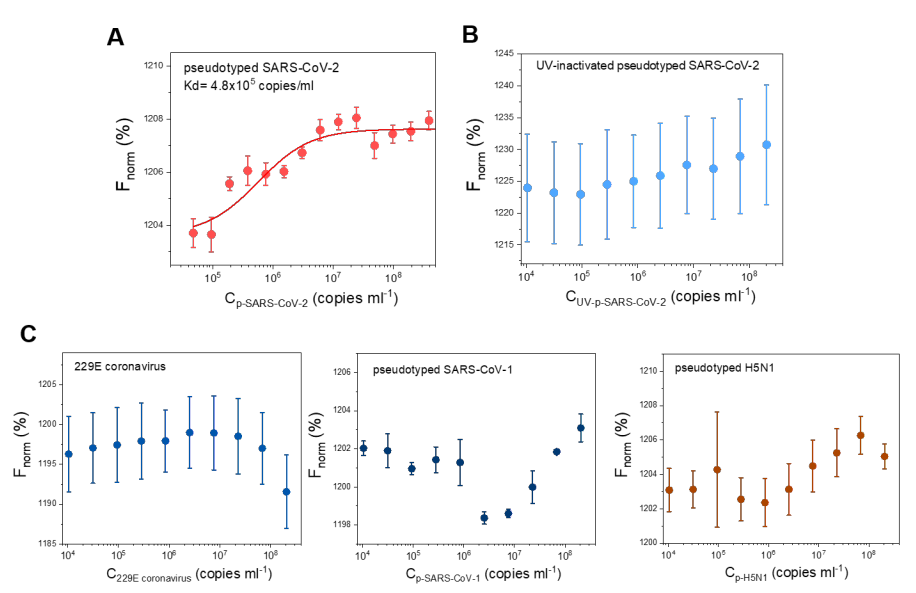


Fig. S15. Binding curves of SARS2-AR10 aptamer and different viruses using MST technique. MST results for: (A) active pseudotyped SARS-CoV-2, (B) UV-inactivated pseudotyped SARS-CoV-2 and (C) other viruses, including 229E coronavirus, pseudotyped SARS-CoV-1, and pseudotyped H5N1. SARS2-AR10 was labeled with FAM at the 5' end and its concentration was fixed at 250nM. These results confirm the binding of the aptamer to active pseudotyped SARS-CoV-2 and its selectivity. n=3 technical replicates (mean \pm SD).

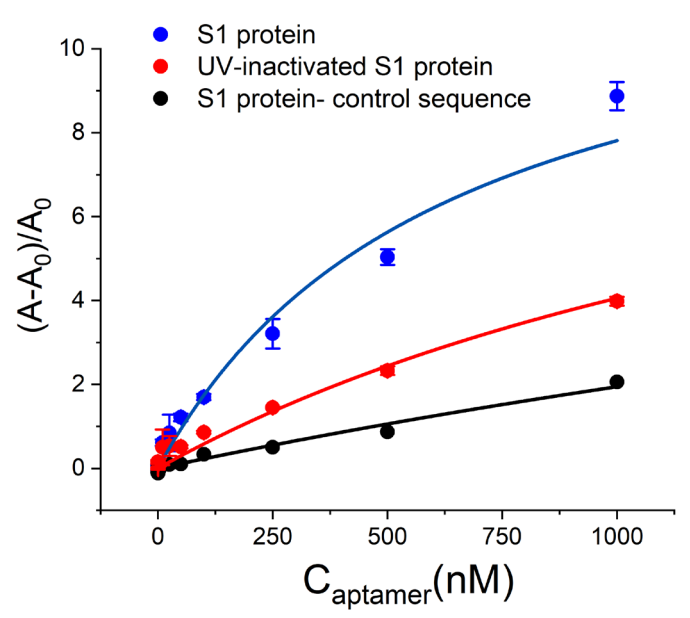


Fig. S16. Binding curves of SARS2-AR10 aptamer and SARS-CoV-2 S1 domain protein obtained by ELONA assay. Blue corresponds to active SARS-CoV-2 S1 domain protein and red to UV-inactivated SARS-CoV-2 S1 domain protein. The dissociation constant, K_d of the SARS2-AR10 aptamer for the active S1 protein is 630 nM, while the affinity to the UV-inactivated protein is lower ($K_d = 2000$ nM). Black corresponds to the ELONA results for the binding of S1 protein to a control sequence. n = 3 technical replicates (mean \pm SD).

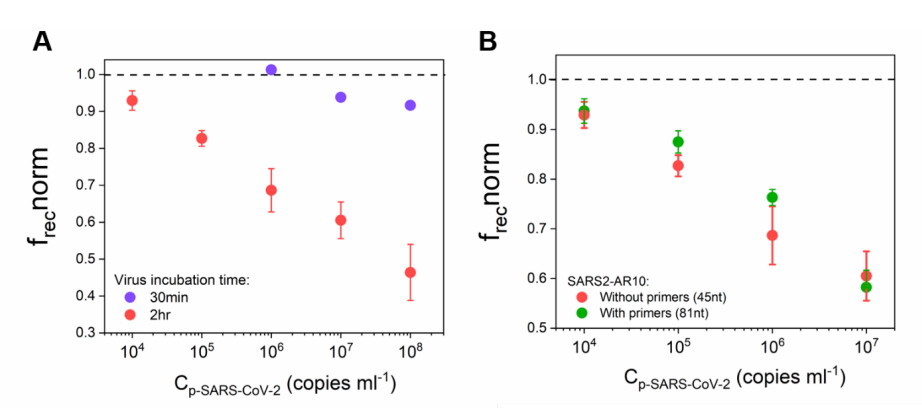


Fig. S17. Effect of virus incubation time and length of the aptamer on the SARS2-AR10-nanopore system performance. (A) Normalized rectification factor versus logarithm of the active pseudotyped SARS-CoV-2 concentration after 30min (purple) and 2hr (red) incubation time of the virus solution with the SARS2-AR10-nanopore system. (B) Comparison of the performance of the SARS2-AR10 with primers (81nt) and without primers (45nt). In both case the performance is comparable, thereby we choose the short version of the aptamer for further application in the nanopore.

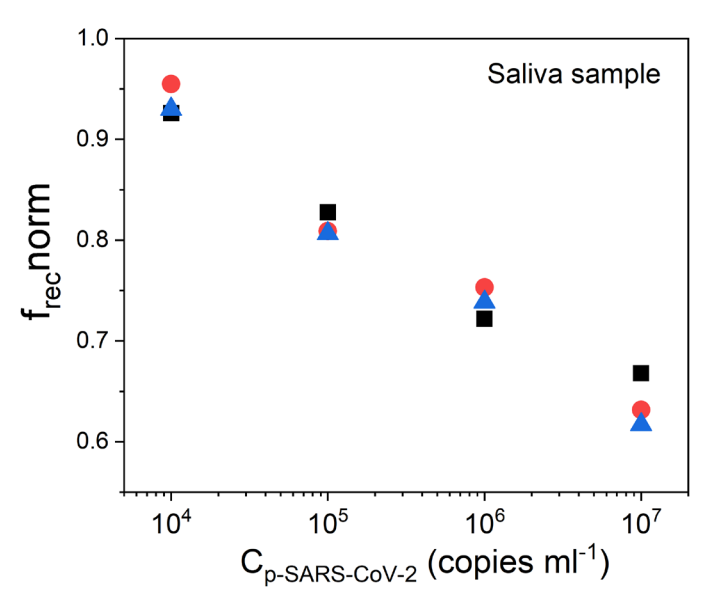


Fig. S18. Detection of active pseudotyped SARS-CoV-2 in saliva samples. Normalized rectification factor versus logarithm of the active pseudotyped SARS-CoV-2 concentration spiked in human saliva sample. A total of 12 saliva samples were spiked with different concentrations of infectious pseudotyped SARS-CoV-2 and each sample was measured with a different nanopore membrane.

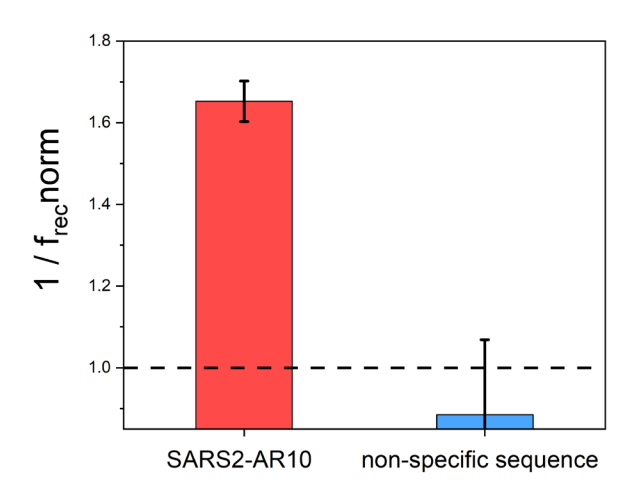


Fig. S19. Comparison of the aptamer-nanopore system signal using SARS2-AR10 aptamer vs using a control sequence. Inverse of the f_{rec} norm obtained for active pseudotyped SARS-CoV-2 (SARS-2) spiked in saliva using SARS2-AR10 aptamer in the nanopores (red) and a control sequence (blue). The concentration of the virus is $1x10^7$ copies/mL. n=3 technical replicates (mean \pm SD).